We are IntechOpen, the world's leading publisher of Open Access books Built by scientists, for scientists

4,800
Open access books available

122,000
International authors and editors

135M
Downloads

Our authors are among the

154
Countries delivered to

TOP 1%
most cited scientists

12.2%
Contributors from top 500 universities

CLARIVATE ANALYTICS BOOK CITATION INDEX INDEXED

WEB OF SCIENCE™

Selection of our books indexed in the Book Citation Index in Web of Science™ Core Collection (BKCI)

Interested in publishing with us?
Contact book.department@intechopen.com

Numbers displayed above are based on latest data collected.
For more information visit www.intechopen.com

5

Radiation Transmission-based Thickness Measurement Systems - Theory and Applications to Flat Rolled Strip Products

Mark E. Zipf
Tenova-I2S (I2S, LLC)
United States of America

1. Introduction

Precise, accurate measurement of strip / sheet thickness is critical in the controlled processing and quality assessment of flat rolled metal products. Through the years, many methods (both contact and non-contact) have been developed, each having specific, relevant applications, and certain characterizable advantages and disadvantages. These systems are provided in a variety of geometries and physical arrangements, and seemingly endless collections of functions and features.

One particular non-contact method employs an understanding of a material's reaction to incident radiation (primarily the photonic / gamma form – although electron / beta radiation can also be considered) in a transmission mode framework. Here, semi-collimated, high energy radiation (a photon beam of a given spectral content) is directed perpendicular to one surface of the flat strip material. Depending on the energy level, the incident radiation interacts with the material's atomic structures and is either passed, absorbed, scattered or involved in high energy pair productions. The resulting transmitted radiation appears as a dispersed beam pattern, having attenuated intensity and modified spectral content. A portion of the exiting radiation is collected by detection instruments which render a signal functionally related to the integral of the received radiation intensity over the detector's spectral bandwidth. Knowledge of the radiation source's intensity and spectral content, the material chemistry and the detector's response characteristics are needed to process the signals and render a thickness measurement.

Typically, the plane of the strip is oriented horizontally with the source and detector mounted above and below the stip. There are a number of different configurations ranging from stationary / physically-fixed source and detector arrangements above and below the strip, to C-Frame / O-Frame mounted configurations that (in some cases) allow for transverse strip thickness profiling, to multi-source / multi-detector arrangements that provide instantaneous measures of the strip profile. Regardless of the physical configuration, the fundamental physics applies.

This chapter is the first of a two-part discussion concerning the nature of radiation transmission-based strip thickness measurement. The intent of this chapter is to examine the underlying physics and methods of this approach, and functions as a tutorial supporting subsequent discussions (Zipf, 2010). Natural and artificial radiation sources are presented and discussed, along with the various means of containing and directing the emitted radiation. The nature of the material's interaction with radiation is analyzed and considered in the presence of possibly complex material chemistries. Detection system sensors and instrumentation are studied and examined with respect to their associated signal processing components and methods of rendering a thickness measurement. Calibration and standardization methods are introduced and combined with the various methods of resolving the material thickness from active measurements. Special functions and features (e.g., transverse profiling, strip quality control, etc.) are discussed and assessed. Classical system architectures and component organizations are presented and considered with respect to typical applications and system implementations.

2. Fundamentals of Non-Contact Radiation Attenuation Gauging

Radiation attenuation gauging involves the measurement of the thickness of a flat sheet of known (or calibrated) material composition, through the assessment of the degree of transmitted attenuation experienced by a beam of high energy ionizing radiation directed perpendicular to the planar surface of the material (I2S, 1992). Figure 2.1 provides a simplified diagram showing the primary concepts and components associated with this approach.

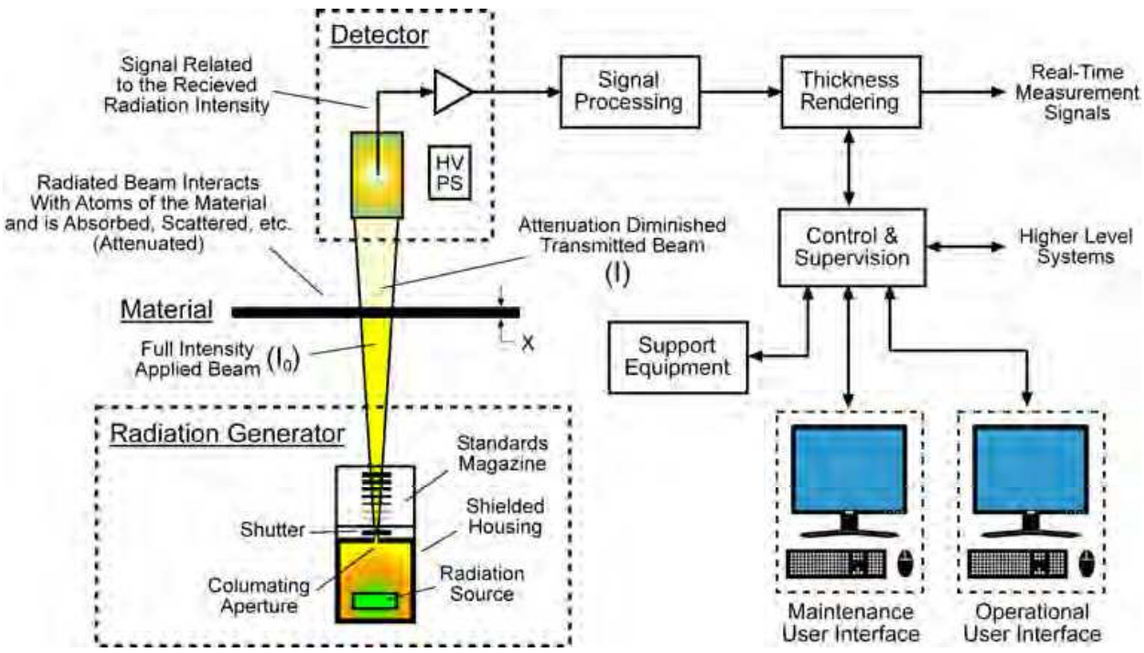

Fig. 2.1 – Diagram illustrating the primary concepts and components associated with transmission-based radiation attenuation gauging.

2.1 General System Objectives and Requirements

Objectives

- Provide a sufficiently accurate, precise, instrumented signal, representative of the measured strip thickness (with accuracy and repeatability < 0.1% of nominal).

Requirements

- Must be "continuous" in nature (not a spot measurement)
- Must measure over a reasonably small surface area (~25mm diameter circle)
- Must provide measurements while the strip is moving (at speed up to 1500 mpm)
- Must be fast responding (5-20msec)
- Must be independent-of or compensate-for alloy variances
- Must compensate for changes in ambient conditions
- Must be highly immune to noise and external interference
- Must not damage the strip surface
- Must provide flexible, multi-facetted interfacing to other systems
- Must provide intuitive, interactive user interfaces (both operational & maintenance)

Desirable Traits

- Measurement of the transverse strip profile
- Insensitive to strip shape / flatness, pass-line height, debris, oil & coolant films, etc.
- Employ Commercial-Off-The-Shelf (COTS) Technologies
- Safe for operational & maintenance personnel
- Physically / mechanically robust
- Real-Time, Interactive, Graphical User Interfaces (GUIs)
- Adaptable, scalable system arrangements & platforms
- Remote Accessibility

2.2 Primary Components

Radiation Generator – This device emits a directed beam of high energy ionizing radiation (of known intensity, I_0 (in photons/sec), and spectral characteristics) and provides radiation containment.

Shielded Housing – This vessel typically consists of a shielded, structural housing containing the associated holders and mounts required to locate and orient the radiation source. The housing may contain dielectric oil immersed components and be supported by an external heat exchanging / cooling system.

Radiation Source – This component generates the radiation that will be applied for measurement. The source may be either natural (radioactive isotope) or artificial (X-Ray tube), and may project a radiation pattern that is sensitive to alignment with the housing aperture.

Collimating Aperture – Radiation is emitted from the housing chamber through a sealed aperture in the form of a beam having a specific, semi-collimated optical geometry needed to support the form and geometry of the application and detector. The aperture is sealed to reduce the infusion of external contaminants and / or the escape of any (possibly pressurized) internally contained dielectric oil.

Shutter - This device provides a means of cutting off the radiation beam, making the radiation generator safe for handling and operations in the proximity.

Standards Magazine - This device contains a group of precision (often NIST traceable) samples that can be introduced into the radiation beam (individually or in groups) to provide a means of measuring the emitted beam's intensity and spectral content for calibration and standardization purposes. (Howard, 1970)

Material Under Measurement – For the purposes of this discussion, we will be considering flat rolled, sheet / strip products, composed of various metals (e.g., steel, aluminum, and copper / brass alloys, etc.) whose width is much larger than the nominal thickness. The strip may be stationary or moving at speeds exceeding 1500 meters/minute.

Detection System – Transmitted / scattered radiation, I (in photons/sec), that results from the incident radiation, I_0, penetrating the strip, is collected and measured by this device, which is typically located above the strip and aligned to the optical axis of the radiated beam. The radiation generator's collimator and detector aperture are sized to provide the detector an optical over-containment of the transmitted beam.

Detector – Collected incident radiation is converted to an electrical signal that is functionally related to the radiation intensity. Ion chambers and scintillation crystal / photomultipliers are often employed (Moore & Coplan, 1983).

High Voltage Power Supply – Detector sensitivity (gain) is related to the applied potential. A high voltage power supply provides the detector potential with sufficient current capacity to provide the necessary charge recovery.

Preamplifier – The feeble detector signal is amplified to usable amplitudes by a high gain, low noise electrometer / transconductance amplifier (Motchenbacher & Fitchen, 1973). To reduce signal noise and interference, it is desirable to place the preamplifier as close as possible to the detector and mounted in a shielded, hermetically sealed enclosure.

Signal Processing – The amplified detector signal requires wide bandwidth signal processing (in both time and amplitude) to render a calibrated measurement of the intensity of the received radiation (i.e., related to material absorption / attenuation). This processing can be provided by discrete electronics and instrumentation, real-time digital signal processors or Field Programmable Gate Arrays (FPGAs).

Thickness Rendering – This subsystem provides the final determination and distribution of the calibrated measurement of strip thickness. Calibration and alloy compensation curves reside in and are supplied by the System Supervisor. The measured thickness is typically transmitted via analog signals or high speed networked numerical data exchanges.

System Supervisor – This subsystem oversees and coordinates the gauging system's control, measurement, calibration and operational activities, along with any operational interfacing to the mill / line control systems.

User and Maintenance Interfaces – Depending on the nature and extent of the system's function, various forms of dedicated operator interfaces may be employed. The user interface can range from simple operator controls and data entry devices, to sophisticated interactive, graphical human machine interfaces (HMIs). The maintenance interface is

typically more sophisticated and provides detailed graphical information concerning the status, activity, calibration and performance data, along with trouble shooting and diagnostic assistance.

Interfaces to External Control and Automation Systems – The gauging system must communicate and interact with the mill / line's related control, automation and high level production systems. Measured thickness indications are often transmitted as analog signals or numerically via dedicated network links. Set-up, operational and status data (i.e., nominal gauge sets, alloy / composition, profile / positioning, shutter, etc) are often exchanged via standard network, serial, or even discrete logic (BCD) interconnects.

3. Ionizing Radiation and Radiation Generators

Radiation is a generalized term used to describe a variety of energy forms that are emitted from a body. For the purposes of this discussion, we will focus on ionizing radiation which involves charged particles or electromagnetic waves possessing sufficient energy to dislodge strongly held electrons from atoms or molecules.

3.1 Forms of Radiation

Ionizing radiation comes in three(3) primary forms: (Halliday, 1955), (Kaplan, 1955)

α-Rays – Alpha radiation involves accelerated helium nuclei, composed of 2 protons and 2 neutrons. This particle has a high mass and a double positive charge. Due to its high mass, this form of radiation has low penetrating energy and a limited range. The primary source of formation is during the nuclear transformation process (radioactive decay), where a new element results.

β-Rays – Beta radiation involves accelerated electrons (or positrons). These particles have a low mass and a negative charge (positive for positrons). Beta rays have modest penetrating energy (more than alpha particles), but can be stopped by metals a few centimeters thick. The primary source of formation is during the nuclear transformation process (radioactive decay), where a neutron is converted to a proton (which remains in the nucleus) and an electron and an antineutrino are emitted. Beta radiation can also be formed by an electron gun in the presence of high electric field potentials.

γ-Rays – Gamma rays are high energy photon emissions (electromagnetic waves) (Kraus & Carver, 1973). Gamma radiation has high penetrating energy and is the primary form of radiation employed in strip thickness gauging systems. X-Rays are also a form of electromagnetic (gamma) radiation. Classically, Gamma Rays and X-Rays have been separated by their respective energy levels (with Gamma being of higher energy). However, a more common place distinction involves the means of their generation. We will examine the various aspects of these differences in the next section.

In fact, there are many forms of radiation (when considering the non-ionizing form), which include: neutron or proton emissions, acoustic, low energy electromagnetic radiation (i.e., thermal, black body, light, radio waves), etc. These forms of radiation are not considered within the scope of this discussion.

3.2 Radiation Sources

Radiation sources are components that generate radiation for application to the measurement process. To limit and direct this discussion, we will focus only on sources that produce high energy photons (electromagnetic waves or γ-Rays). Although β-Ray sources are common, a vast majority of the industrial applications employ γ-Ray emissions. As noted previously, it is necessary to draw specific distinctions between the forms of electromagnetic radiation, under consideration, in terms of their origins.

3.2.1 Naturally Occurring Gamma Rays (Isotope Sources)

Naturally occurring gamma rays are specifically produced by radioactive isotopes during the nuclear transformation process, where following the emission of alpha and / or beta radiation, the decaying nucleus releases excess energy (in the form of photons) to obtain an equilibrium (Halliday, 1955), (Kaplan, 1955). These photon emissions form very well defined spectral lines at specific energy levels and relative amplitudes (Halliday, 1955), (Graydon, 1950). Common radioactive isotopes are: Americium 241, Cesium 137, Curium 244. Figure 3.1 shows the spectral characteristics of photonic radiation released by the radioactive isotope Americium 241.

Primary Radiation			
Type	Energy	Unit	Relative Intensity
Alpha	5443	(keV)	84.5
	5485	(keV)	13
Beta	52	(keV)	< 1
Gamma	**13.9**	(keV)	**42**
	26.3	(keV)	2.4
	59.5	(keV)	**35.9**

(a)

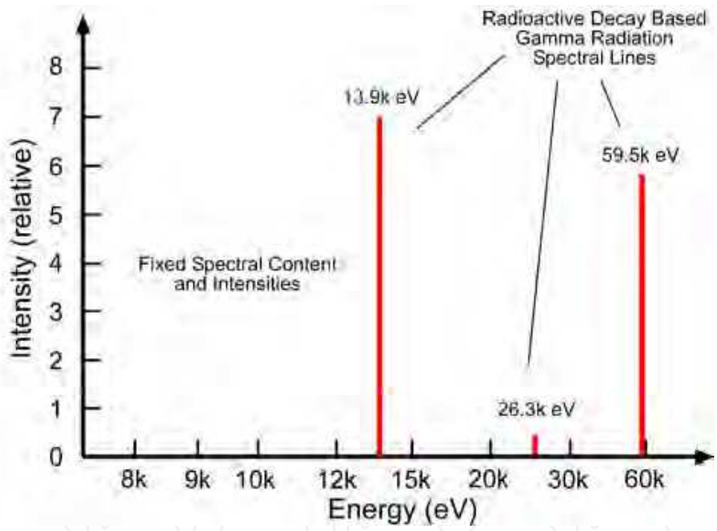

(b)

Fig. 3.1 – Spectral characteristics of the radioactive isotope Americium 241: a) Table defining the form of radiation emitted, the energy level and relative intensity, b) Spectral characteristics of the Gamma radiation components.

3.2.2 Artificially Produced Gamma Rays (X-Ray Sources)

X-Rays (in this context) are specifically generated by high energy, inbound electrons interacting with the inner shell electrons of an atom or the atom's electric fields. These interaction processes, shown in Figure 3.2, produce two distinctly different spectral emissions.

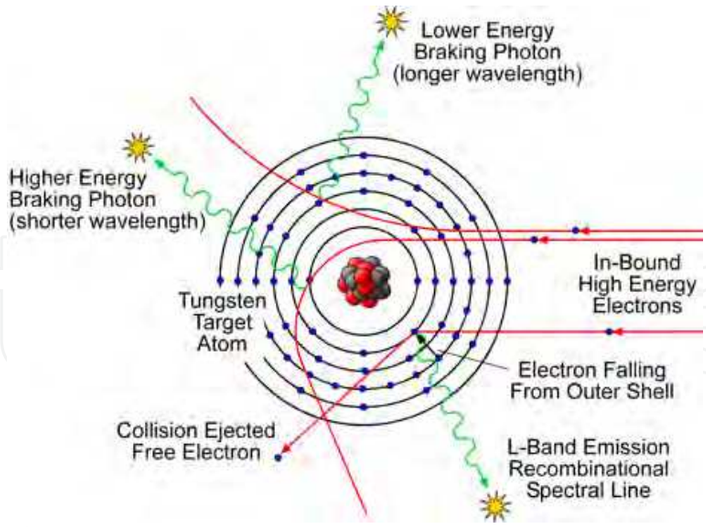

Fig. 3.2 – Nature of X-Ray generation via high energy electron interaction with a Tungsten atom based on a Bohr atomic model of the inbound electron interaction.

Characteristic Spectral Lines – Here an inbound high energy electron has sufficient energy to dislodge an atom's inner shell electron, to the extent of either lifting it to an outer shell (excited state) or removing it from the atomic union (ionized state). The shell's vacated electron position is filled (almost immediately), by a loosely bound electrons from the outer shells, resulting in a release of energy (in the form of a high energy photon), corresponding to the binding energies of the shells involved. The energy released produces discrete, well defined recombinational spectral lines (Mark & Dunn, 1985). The general characteristics of these spectral lines are shown in Figure 3.3 for Tungsten.

Bremsstrahlung Spectra – This spectral content develops when high kinetic energy electrons encounter the electric fields of the atom and are either decelerated or deflected from their previous trajectories (Halliday, 1955). The kinetic energy lost during this deceleration / deflection is emitted as electromagnetic radiation. An electron's inbound kinetic energy can be dissipated as X-Rays either entirely (in a single-stage nucleus encounter) or by several multi-stage encounters, each causing a different radiated energy. When an electron passes-by / interacts-with an atom, the proximity of its trajectory to the nucleus plays a direct role in the amount of energy dissipated. The probability of radiated energy dissipation elevates as the distance from the nucleus increases (i.e., larger distances from the nucleus induce weaker / more frequent radiation events, while shorter distances from the nucleus cause stronger / less frequent radiation events). The spectral content (shown in Figure 3.3) of the Bremsstrahlung component is not a discrete line spectra, but a continuum spanning the initial kinetic energy of the inbound electron (i.e., the maximum spectral energy equals the original kinetic energy of the electron) (Mark & Dunn, 1985).

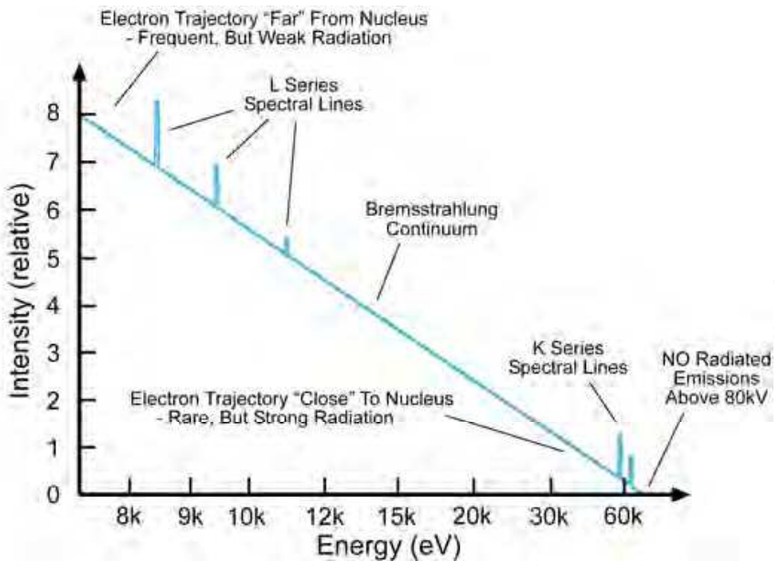

Fig. 3.3 – Spectral characteristics of an 80kV electron beam bombarding and interacting with the atoms of a Tungsten target.

3.3 Radiation Generation

The Radiation Generator emits a directed, collimated beam of high energy ionizing radiation and provides protective radiation containment. When considering isotope source based radiation generators, these devices are very simple (I2S, 1992). They contain only a shielded housing, an isotope source cartridge / pellet, source holder, columating aperture and a shutter. Due to the rather simplistic nature of these generators, we will forgo discussing their associated details.

3.3.1 X-Ray Generators

X-Ray source based radiation generators are far more complex than their isotopic counterparts. In the most classical sense, X-Ray generators are based on the components shown in Figure 3.4 and discussed in the following:

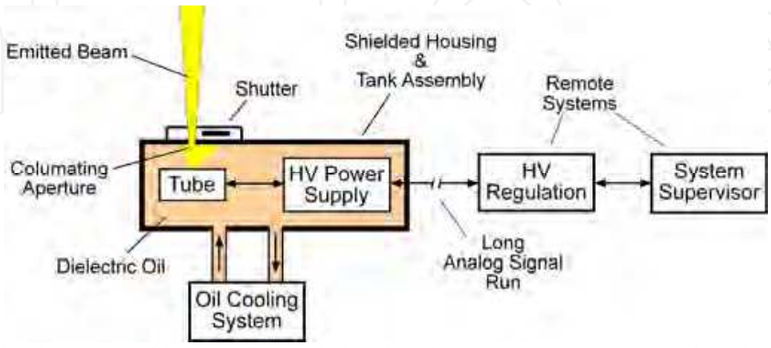

Fig. 3.4 – Block diagram illustration of the basic components associated with an X-Ray Generator.

X-Ray Tube – An X-Ray tube is a vacuum tube that when energized emits a polychromatic gamma ray spectrum (Howard, 1970), (Moore & Coplan, 1983). The spectral range is a direct function of the applied tube potential, and the intensity of the radiation is a direct function of the applied tube current. Figure 3.5 provide a diagram showing the primary components of an X-Ray tube.

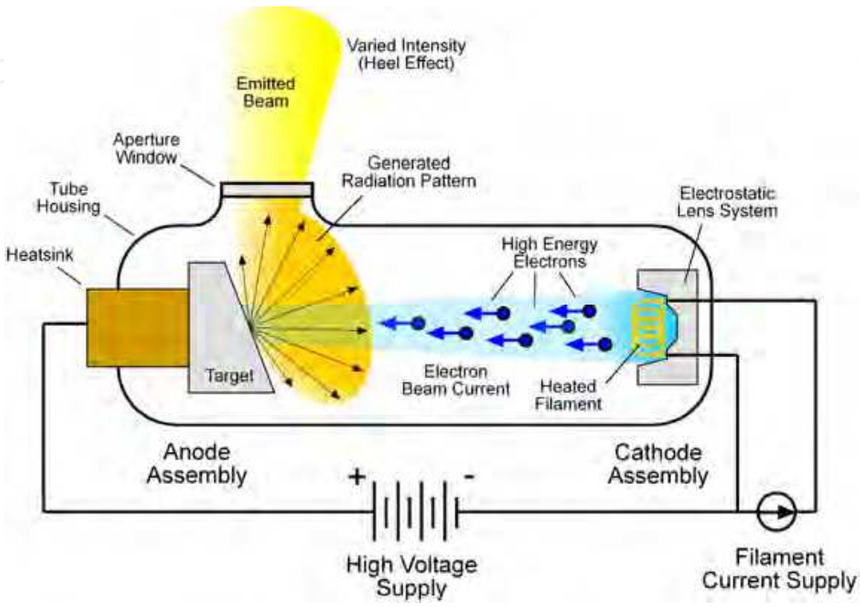

Fig. 3.5 – Simplified diagram showing the basic components of an X-Ray Tube.

Tube Housing – The tube is typically constructed of a sealed, cylindrical glass or ceramic housing and maintains a vacuum. Depending on the aperture material / mounting arrangement and the anode heat sink configuration, the tube geometry may have extensions or added structures, and can be shrouded by a circulating fluid heat exchanger cooling jacket.

Filament – This (typically) Tungsten coil is heated by a constant current source to temperatures that cause sufficient thermal excitation of the valence shell electrons to escape their atomic bonds and form a "cloud" of free electrons.

Target – This (typically) Tungsten plate emits polychromatic X-Rays when its atoms are bombarded by a beam of high kinetic energy electrons. The target's active surface is typically angled to direct the radiation pattern toward the tube's aperture. The angle must be optimized to provide the desired radiation intensity while still maintaining a concentrating projection of the applied electron beam pattern.

High Voltage Power Supply and Tube Potential – A high voltage, direct current (DC) power supply (often 10kV to 200kV) applies a precision regulated, potential between the filament (cathode) and the target (anode), to draw free, thermally excited electrons from the filament and accelerate them to their target impact energy, forming an electron beam. The beam's charge displacement forms a current across the tube (beam current). The power supply's current limits regulate the applied current / tube power. The high voltage electronics /

equipment is often immersed in a dielectric oil bath to provide insulation and allow for a more compact design. The high voltage power supply control and regulation are often provided by external equipment, possibly remotely located.

Electrostatic Lens – The geometric arrangement of this component forms electric field patterns that focus the electron beam to a specific target impact spot geometry (Harting & Read, 1976). Figure 3.6 provides an illustration of the formed electric field lines, and their impact on the electron trajectory.

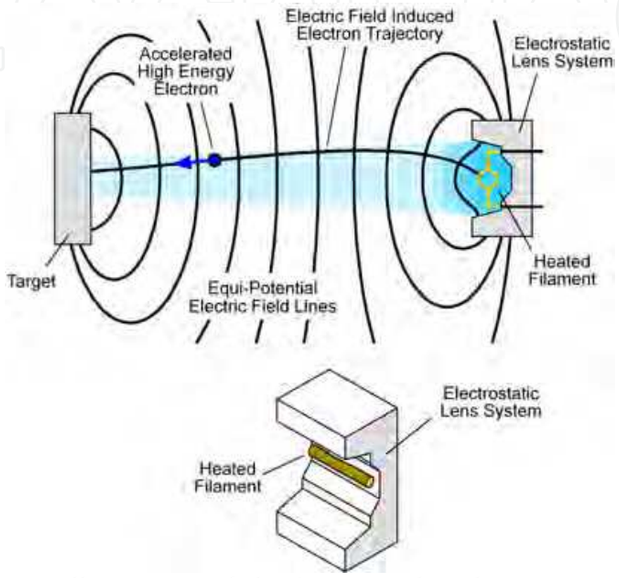

Fig. 3.6 – Block diagram illustration of the X-Ray Tube Electrostatic lens induced electric field lines and associated electron trajectory.

Dielectric Oil – The X-Ray tube and the high voltage power components are often immersed in an oil bath to provide both a high degree of electrical insulation and also a tube heat dissipation capacity.

Thermal Considerations – X-Ray tubes are highly inefficient, with only about 1% of the applied power being converted to X-Ray production. The remainder is converted to heat. Industrial X-Ray tubes are often immersed in an oil bath to dissipate the tube's thermal power. Depending on the tube power and the nature of the generator's housing, the generated heat may exceed the passive dissipation capabilities, thereby requiring an external, oil circulating, cooling / heat exchanging system.

Radiation Pattern and Heel Effect – The target's emitted radiation pattern is dependent on the angular orientation of the target and the spot-size / geometry of the electron beam. Figure 3.7 provides insight into the nature of these radiation patterns and heel effects. The lobed radiation pattern is caused by the angle at which the photons emerge from beneath the surface of the target at the focal point. This causes a differential attenuation of the photons that will ultimately compose a useful, emitted beam. The resulting radiation pattern emitted through the tube's aperture has radial / transverse variations in intensity (often termed "heel effect"), (Mark & Dunn, 1985).

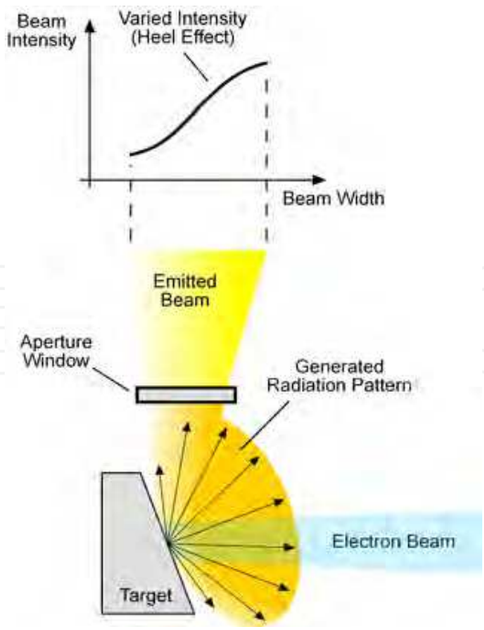

Fig. 3.7 – Illustration showing the varied intensity of the emitted beam associated with the geometry of the target, radiation pattern and location of the tube aperture window.

Tube / Tank Assembly – This component of the generator housing provides a sealed vessel in which the dielectric oil bath is contained and the tube / high voltage power components are mounted. This assembly typically utilizes a lead intermediate liner for radiation shielding and often employs an insulating inner liner (e.g., polypropylene).

Collimating Aperture – The geometry and location of this aperture (with respect to the X-Ray tube mounting and radiation pattern) defines the optical geometry and uniformity of the X-Ray generator's emitted beam. The aperture material will impact the radiated spectrum through energy dependent absorption and scattering processes. Depending on the nature of the tube / tank assembly and shielded housing, the aperture may be required to provide a fluid pressure seal to prevent dielectric oil seepage.

Shutter – A retractable shutter (typically lead) provides the ability to suppress the X-Ray generator's emission, while still allowing the X-Ray tube to be energized (often the tube is kept active to maintain a thermal equilibrium).

System Supervisor – This system component provides the desired references for the tube potential, beam current and filament current, and monitors the tube / tank status, temperature, etc. to control and oversee the generator's operations and performance.

Spectral Characteristics of the Tube / Generator Emitted Radiation – Within the X-Ray tube housing, the polychromatic spectral content of the produced radiation is based on the target material's characteristic and Bremsstrahlung spectra (see Figure 3.3). Beyond the tube's aperture and the aperture of the generator's collimator, the spectral content is modified by the absorption and scattering behavior of the aperture materials (possibly fused silica, calcium fluoride, beryllium, polypropylene, etc.) and any intervening dielectric oil. This causes an attenuation of the lower energy regions of the emitted spectrum (see Section 4.2

concerning the energy dependencies of the Mass Attenuation Coefficient). The resulting spectrum contains a higher energy content, making the beam more penetrating (harder). Figure 3.8 provides example plots of spectral content of Tungsten target radiation attenuated by a glass window aperture for differing applied tube potentials.

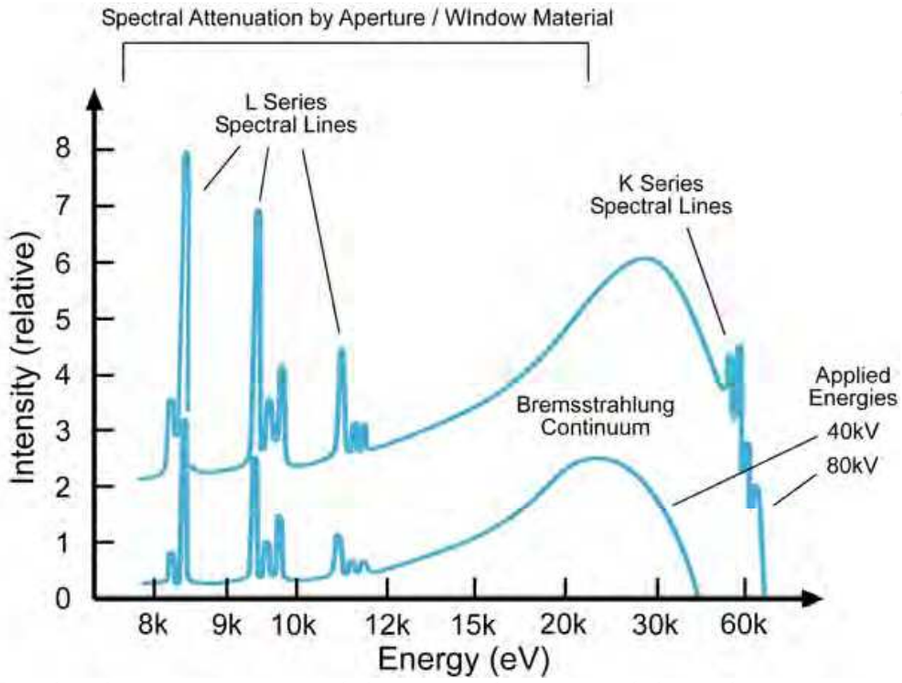

Fig. 3.8 – Graphical representations of the spectral content of the radiation emitted from a Tungsten target X-Ray tube with a glass aperture window, showing the Characteristic and Bremsstrahlung radiation spectrum for 80kV and 40kV tube potentials.

The key feature of this spectrum is the significant attenuation by the aperture window of the lower energy region (as noted by the diminished region of Bremsstrahlung radiation below 20kV). It is important to note that the lower tube potential (40kV) does not provide an electron beam with sufficient kinetic energy to dislodge the target material's K shell electrons (indicated by the lack of K Series recombinational spectral lines).

Controlled Variability of Tube / Generator Emissions – By varying the applied tube potential and beam current, the radiated tube / generator spectral content and intensity can be adjusted to meet the needs of the measurement application. Figures 3.9 and 3.10 show the reactions of the Bremsstrahlung radiation spectra to changes in the tube potential and beam current, respectively.

Beam Hardening – This term traditionally describes the process of increasing the average energy of the emitted spectrum. This causes the resulting beam to have a greater penetrating capability. Beam hardening can be achieved through the used of selected pre-absorbers, whose spectral attenuation characteristics suppress lower energy regions (compare Figures 3.3 and 3.8). This beam hardening effect can also be formed by increasing the applied tube potential. As shown in Figure 3.9, increasing the tube voltage causes the emitted spectrum's peak intensity to shift to higher energies.

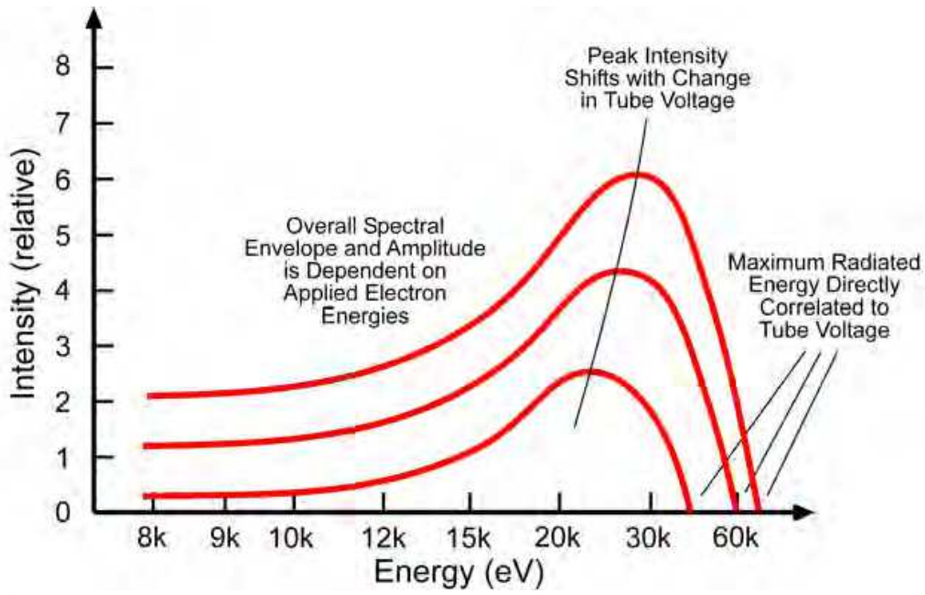

Fig. 3.9 –Illustration of the Bremsstrahlung spectra behavior due to variations in the applied tube potential, while maintaining a constant beam current. This illustrates that an increase in the tube voltage causes a beam hardening effect, by shifting the spectrum's average energy to higher (more penetrating) levels.

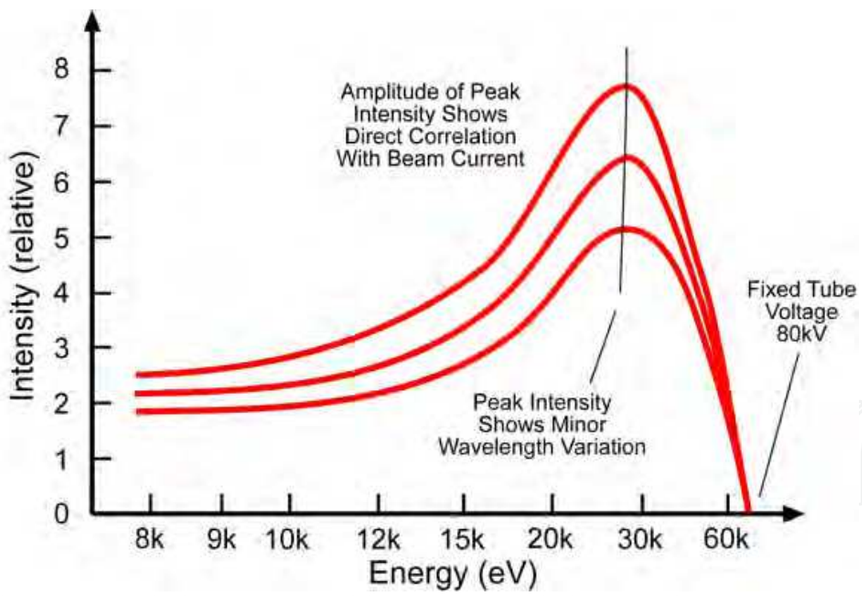

Fig. 3.10 –Illustration of the Bremsstrahlung spectra behavior due to variations in the applied beam current, while maintaining a constant tube potential.

4. Interaction of Radiation with Materials

The collimated beam of radiation emitted by the radiation generator is directed (typically perpendicular) to one surface of the material. The incident radiation interacts with the

material's atomic structures and is either passed, absorbed, scattered or involved in high energy pair productions. The nature of this interaction is dependent on the spectral energy content of the applied radiation and the composition of the material. The resulting transmitted radiation appears as a dispersed beam pattern, having attenuated intensity and modified spectral content.

4.1 Attenuation Effects Based on Form of Radiation

The nature of the material interaction is dependent on the form and energy content (wavelength) of the inbound radiation. A number of processes are involved (e.g., collision, photoelectric absorption, scattering, pair production) and their cumulative effect can be characterized as an energy dependent attenuation of the intensity, and a modification of the radiated pattern of the transmitted beam (through scattering processes) (Kaplan, 1955), (Letokhav, 1987).

α-Particles – Due to their dual positive charge and their relatively large mass, Alpha particles interact strongly (through collision processes) with the material's atoms and are easily stopped (Kaplan, 1955).

β-Particles – Due to their physical mass and negative charge, Beta particles also interact through collision / scattering processes. Elastic and inelastic scattering processes are associated with manner in which inbound, high energy electrons interact with the electric fields of the material's atoms (Kaplan, 1955), (Mark & Dunn, 1985).

Inelastic Scattering – A certain amount of the inbound radiation energy is dissipated through an ionization or excitation of the material atoms. Here, the inbound energy is sufficient to dislodge electrons from their shells, forming an ion, or shell electrons are excited to outer shells. Recombinational gamma spectra (electromagnetic) is produced and radiated in all directions, when the excited or ionized electrons fall into the inner shells.

Elastic Scattering – This lesser (secondary) radiation tends to possess lower energy content and is also radiated in all directions. The radiation intensity is an increasing function of the material's atomic number. This attribute is well suited for measuring coating thicknesses on base materials (having different atomic numbers to the coating) via backscattering techniques.

γ-Rays – Gamma rays (electromagnetic energy) are attenuated through reductions in their quanta energies, via the combined processes of photoelectric absorption, scattering and pair production (Hubble & Seltzer, 2004). The experienced attenuation is an exponential function of the inbound radiation energy spectra, and the material composition and thickness. This relationship makes this form of radiation an attractive choice for material thickness measurement via a knowledge of the applied radiation, the material composition and an examination of the resulting transmitted radiation.

4.2 Mass Attenuation Coefficient

The manner in which a composite / alloyed material responds to inbound photonic radiation can be characterized by the composite Mass Attenuation Coefficient (MAC), μ/ρ, of its elemental constituents (typically with units of (cm^2/g)). The MAC is a material density

normalization of the Linear Attenuation Coefficient (LAC), μ, where ρ is the density of the material (in g/cm^3), and the MAC is therefore an energy dependent constant that is independent of physical state (solid, liquid, gas). The reciprocal of the LAC, q, is often termed the Mean Free Path. The MAC is typically characterized as an energy cross-section, with the amplitude of attenuation being a function of applied photonic energy, (Hubble & Seltzer, 2004). Figure 4.1 provides a graphical representation of the MAC for the element Iron (Fe, Atomic No.: 26). Radiation attenuation is composed of five(5) primary processes:

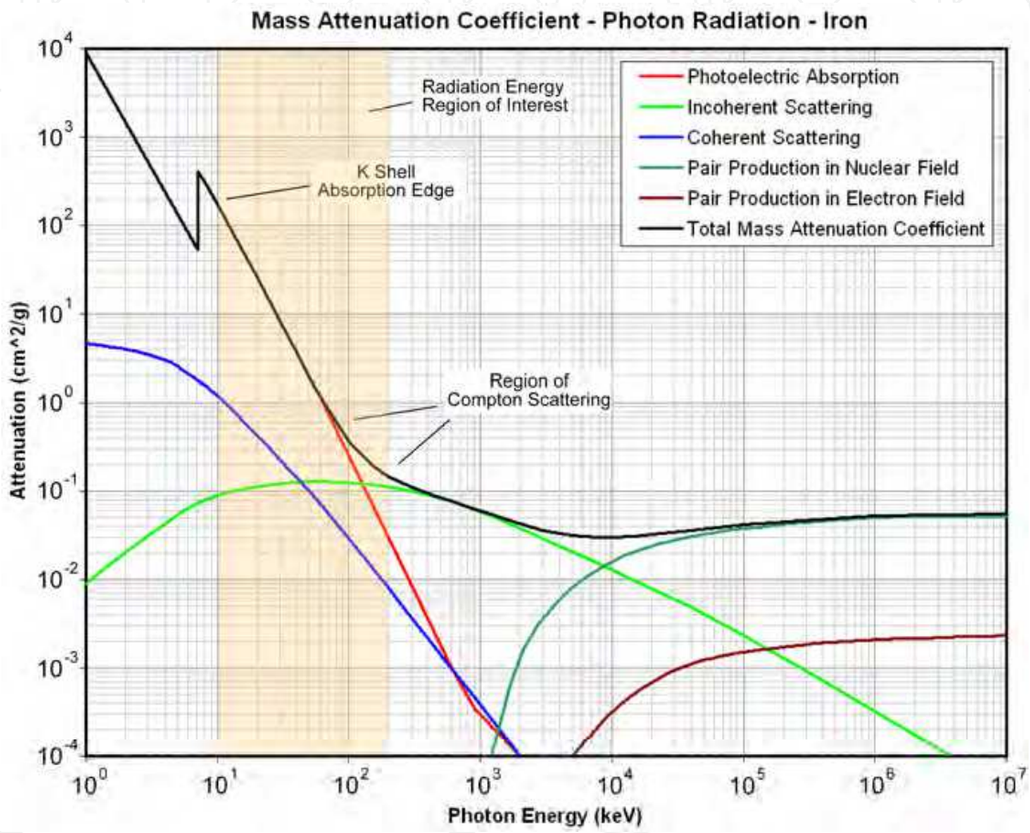

Fig. 4.1 – Graphical representations of the Mass Attenuation Coefficient, (μ/ρ), of the element Iron (Fe) as a function of the applied photonic energy.

Photoelectric Absorption – This process is in effect at lower energies and involves the conversion of the inbound photon's energy to the excitation of the material atom's inner shell electrons (K or L), beyond their binding energies and dislodging them from the atom, to form an ion (Mark & Dunn, 1985). These free electrons (photoelectrons) recombine with free ions and radiate with a characteristic spectra of the material's constituent atoms (recombinational spectral lines). This radiation is emitted in all directions in the form of an X-Ray fluorescence (whose energy increases with atomic number). If the inbound radiation energy is below shell's binding energy, photoelectrons are not formed from that shell and an abrupt decrease in the material's absorption characteristics is noted (see the abrupt, saw-tooth absorption edge in Figure 4.1).

Incoherent Scattering (Compton Scattering) – This absorption process is in effect over a broad range of energies, and involves inelastic scattering interactions between the material atom's electrons and the inbound photonic radiation (Kaplan, 1955). The electrons are transferred part of the inbound radiation energy (causing them to recoil) and a photon containing the remaining energy to be emitted in a different direction from the inbound, higher energy photon. The overall kinetic energy is not conserved (inelastic), but the overall momentum is conserved. If the released photon has sufficient energy, this process may be repeated. The Compton scatter radiation has a directional dependency that results in radiated lobes of having angular intensity dependencies.

Coherent Scattering (Rayleigh Scattering) – This absorption process is in effect in the lower energy regions, and involves the elastic scattering interactions between the inbound photons and physical particles that are much smaller than the wavelength of the photon energy, (Kaplan, 1955).

Pair Production – This absorption process is in effect only at very high energies (greater than twice the rest-energy of an electron (>1.022MeV)), and involves the formation of electron pairs (an electron and a positron), (Halliday, 1955). The electron pair converts any excess energy to kinetic energy, which may induce subsequent absorption / collisions with the material's atoms. This absorption process occurs only at very high energies, and therefore has no practical application in the forms of thickness measurement considered here.

The summation of these components forms the MAC and precision cross-section data is openly published as tabulated lists by the National Institute of Standards and Technology (NIST) (Hubble & Seltzer, 2004), for all the naturally occurring periodic table elements to an atomic number of 92 (Uranium).

It is important to examine the nature of the material absorption characteristics within the region of radiation energy of interest (10keV – 200keV), see Figure 4.1. Here, the attenuation characteristics of the lower energy section is dominated by the Photoelectric absorption. At energies higher than about 100keV, Compton Scattering becomes the primary method of attenuation.

Depending on the nature of a given element's atomic structure and atomic weight, the behavior of the MAC can vary widely. Figure 4.2 provides a comparative plot of four common elements, along with an indication of the energy level associated with the primary spectral line for Americium 241 (59.5keV). The key aspect of this comparison is the extent and energy regions involved in the differences in the attenuation characteristics. Carbon offers very little attenuation and only at low energies, while lead dominates the spectrum, especially at higher energies, illustrating its excellent shielding characteristics. Copper and iron have very similar behavior, and also show K Shell absorption edges at their distinct energies. The differences in attenuation between these metals appear to be relatively small, however, in the region about 60keV, copper has over 30% more attenuation than iron.

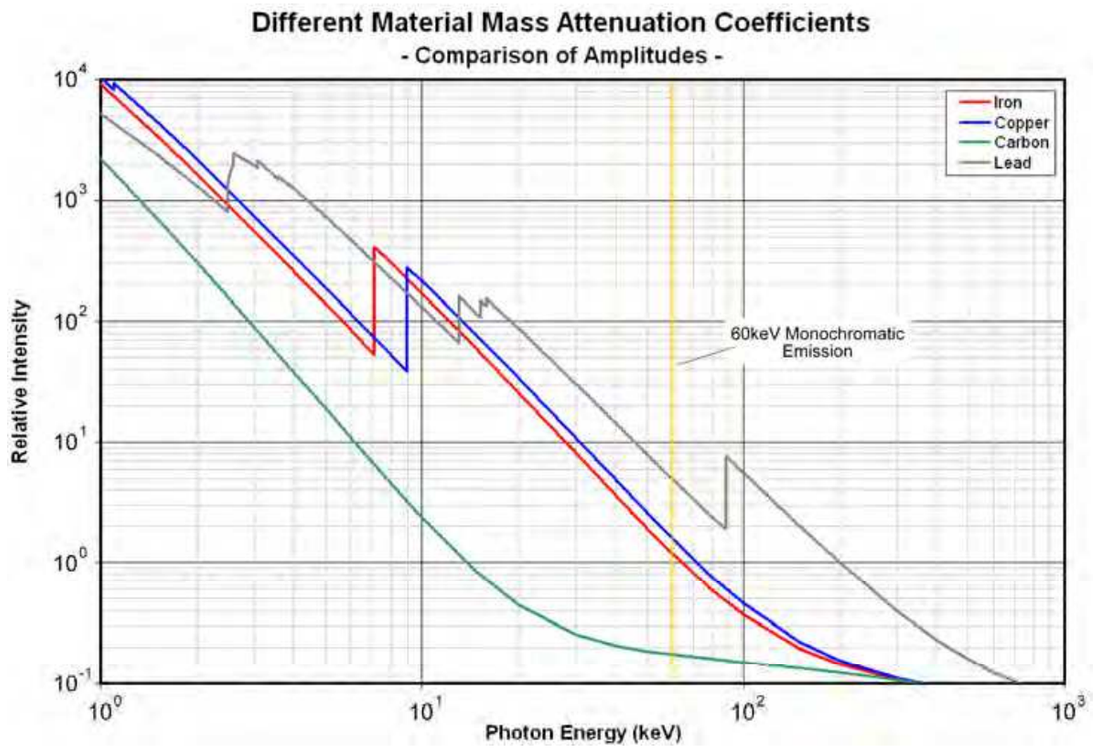

Fig. 4.2 – Graphical comparisons of the energy dependent MACs of differing materials and an indication of the location of 60keV incident radiation.

4.3 Attenuation Characterization

4.3.1 Monochromatic Beer-Lambert Law

When monochromatic radiation of known intensity, I_0, is attenuated by the material, the relationship to the resulting, transmitted radiation, I, is an exponential function of the MAC, the material density and thickness, originating from the differential form:

$$-\frac{dI}{I} = \mu\, dx = \frac{dx}{q} \tag{4.1}$$

where

μ – Linear Absorption Coefficient (LAC - subject to material density variations)
q – Mean Free Path (MFP – subject to density material variations)
x – Material Thickness

Integrating Eq(4.1) results in:

$$I = I_0\, e^{-\mu x} = I_0\, e^{-\frac{x}{q}} \tag{4.2}$$

Expanding Eq(4.2) to employ the MAC, , produces the Beer-Lambert Law (Halliday, 1955), (Kaplan, 1955):

$$I = I_0 e^{-\left(\frac{\mu}{\rho}\right)\rho x} = I_0 e^{-\frac{x}{q}} \tag{4.3}$$

where

$\left(\mu/\rho\right)$ – Mass Attenuation Coefficient (MAC), (cm^2/g)

ρ – Material density (g/cm^3)

Figure 4.3 provides a graphical relations showing the nature of the exponential attenuation characteristics of a monochromatic incident radiation as a function of material thickness in terms of multiples of the material's MFP.

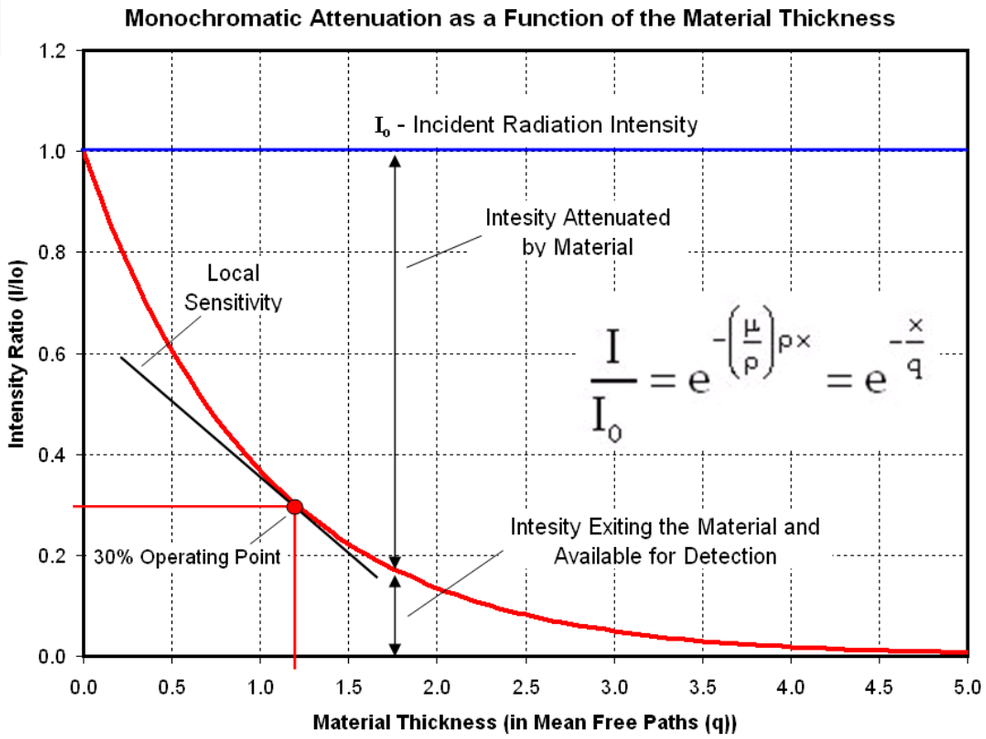

Fig. 4.3 – Monochromatic exponential attenuation as a function of material thickness in terms of multiples of the material's Mean Free Path (q).

4.3.2 Attenuation in Composite Materials

When a material is formed by a combination of constituents (e.g., alloy), the weighted inclusion contributions of the individual components must be taken into account. The composite material's MAC is given by (Hubble & Seltzer, 2004):

$$\left(\frac{\mu}{\rho}\right)\rho = \sum_{i=1}^{N} w_i \left(\frac{\mu}{\rho}\right)_i \rho_i \tag{4.4a}$$

$$\left(\frac{1}{q}\right) = \sum_{i=1}^{N} \left(\frac{w_i}{q_i}\right) \tag{4.4b}$$

where

$\left(\mu/\rho\right)_i$ – The MAC of the i[th] constituent, of N total constituents

w_i – The decimal percentage of inclusion of the i[th] constituent

$$\sum_{i=1}^{N} w_i = 1.0 \tag{4.5}$$

The single element relationship of Eq(4.3) is therefore extended to the composite material:

$$I = I_0 e^{-\sum_{i=1}^{N}\left(w_i\left(\frac{\mu}{\rho}\right)_i \rho_i\right)x} \tag{4.6}$$

4.3.3 Polychromatic Dependencies of Attenuation

The Beer-Lambert Law of Eq(4.3) (and Eq(4.6)) applies only to monochromatic radiation energy, however, typical radiation sources rarely emit purely singular energies (note the spectral content shown in Figures 3.1b and 3.6a. It is therefore necessary to extend the relationships Eq(4.3) and Eq(4.6) to include the polychromatic spectral content of the applied and transmitted radiation, along with the energy cross-section of the MAC. This is provided through the inclusion of the wavelength (energy) dependency of these components.

$$I(\lambda) = I_0(\lambda) e^{-\left(\frac{\mu}{\rho}(\lambda)\right)\rho x} = I_0(\lambda) e^{-\frac{x}{q(\lambda)}} \tag{4.7}$$

The use of wavelength, as opposed to energy is purely for convenience, and Eq(4.7) can be extended to include the effects of composite materials, Eq(4.4) and Eq(4.6). Figure 4.4 provides graphical examples of how the incident radiation amplitude and polychromatic spectral content is attenuated / modified by its interaction with material. It's interesting to note that manner in which lower energy region attenuating characteristics of the material under measurement causes a beam hardening effect on the radiation available to the detector (note the higher average energy level in Figure 4.4b compared to 4.4a).

5. Radiation Detection / Measurement

Attenuated / scattered, polychromatic radiation, I(λ), that results from interaction with the material, is collected and measured by a detector aligned with the optical axis of the generator's radiated beam and has an aperture sized to over-contain the transmitted beam. The detector produces a signal that is functionally related to the total received, polychromatic radiation energy within the spectral bandwidth of the detector's sensitivity.

$$I_D \sim \int D(\lambda)\, I_0(\lambda) e^{-\left(\frac{\mu}{\rho}(\lambda)\right)\rho x} d\lambda = \int D(\lambda)\, I_0(\lambda) e^{-\frac{x}{q(\lambda)}} d\lambda \tag{5.1}$$

where

I_D – The detector's response / measurement signal

$D(\lambda)$ – The detector sensitivity (a function of wavelength / energy)

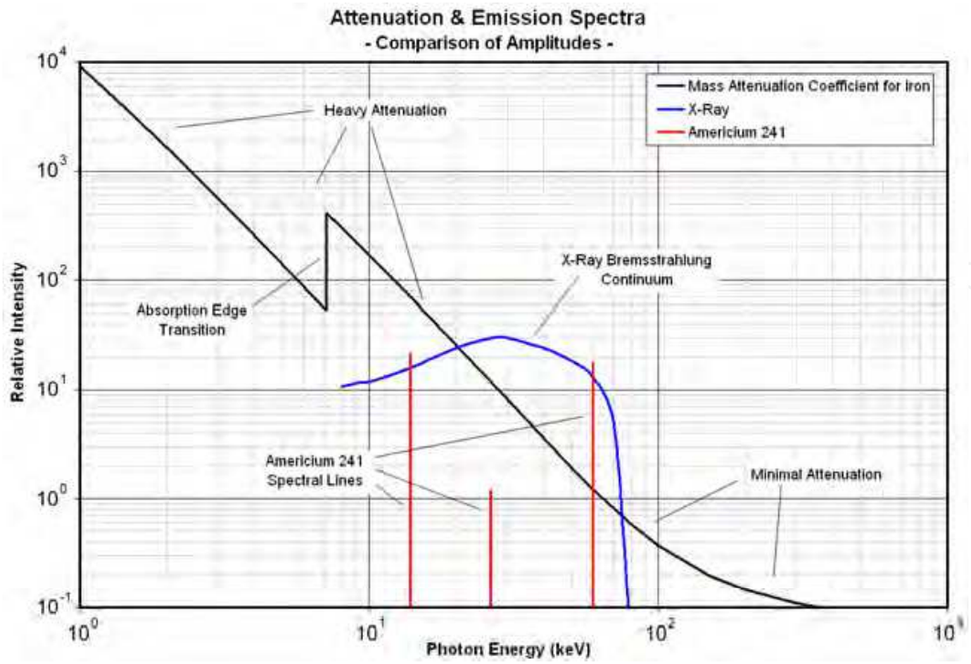

(a)

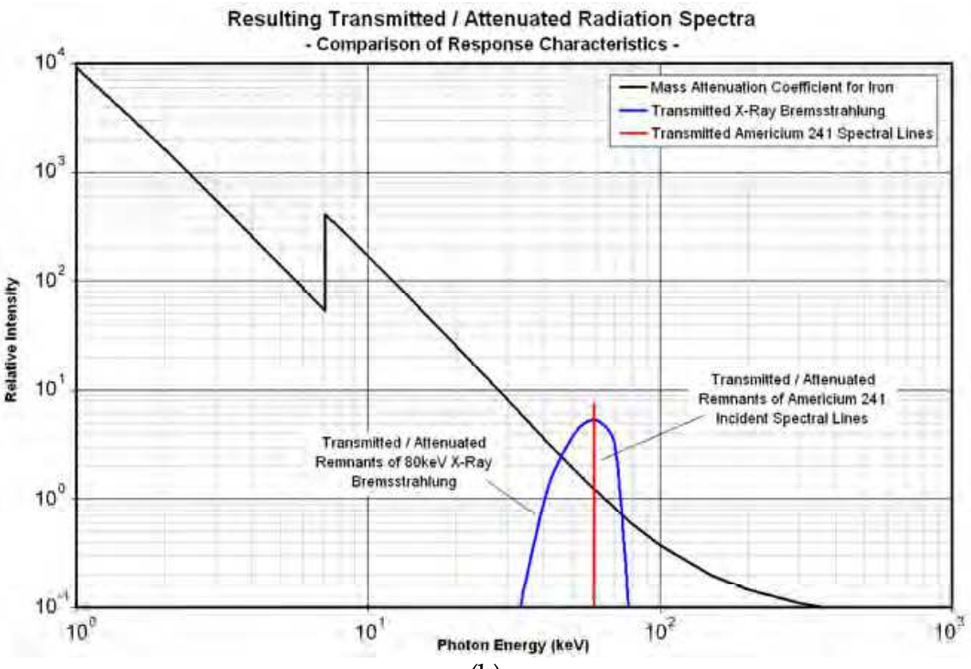

(b)

Fig. 4.4 – Graphical before-and-after comparison of the amplitude and polychromatic spectral modifications of differing sources of incident radiation's interaction with material: a) MAC cross-section of Iron overlaid with the inbound spectral content of both the Americium 241 spectral lines and 80keV X-Ray Bremsstrahlung radiation, b) Transmitted / attenuated spectral content resulting from material interaction.

There are many types of detectors, and we can generally classify them in terms of the nature of their responses to incident radiation.

Ionization Methods – This includes a large class of detectors that respond to incident radiation as a function of the level of ionization occurring within them (Moore & Coplan, 1983). These include: ion chambers, proportional counters, Gieger-Muller counters, cloud chambers, spark chambers, fission chambers and certain semiconductor devices.
Molecular Excitation and Dissociation Methods – This includes detectors that respond to incident radiation as a function of the molecular excitation and dissociation, along with a certain degree of ionization (Moore & Coplan, 1983). These include: scintillation counters, chemical dosimeters and optical properties based systems.

To narrow the focus of this discussion, we will focus on the examinations of ion chamber and scintillation based detectors.

5.1 Ionization Chamber Detectors

Ionization chambers (ion chambers) consist of a media (usually gas) filled chamber containing two(2) charged electrodes, (Halliday, 1955), (Kaplan, 1955), (Moore & Coplan, 1983). The chamber aperture may consist of a sealed window made of a material that either efficiently passes or possibly attenuates the incident radiation, depending on the planned range of radiation intensity. The chamber geometry is typically organized to accommodate the application, generally in the form of a cylindrical arrangement.

5.1.1 Ionization Processes

Depending on the intended radiation form, photons or other charged particles (neutrons, electrons, etc.) enter the chamber aperture and transit through the media, where they interact with the atoms forming the media. Depending on the circumstances, these interactions can strip-away electrons from the outer shells of the media, thereby forming ion / free-electron pairs (ion pairs), via direct or indirect ionization processes. The energy required to form an ion pair is often termed the ionization potential (which is typically on the order of 5-20eV) (Graydon, 1950), (Letokhav, 1987).

Direct Ionization – Charged particles (alpha or beta) passing through the media may either collide with the electrons of media atoms, and impart sufficient kinetic energy eject them from the atom, or they may transfer sufficient energy by their interactions with the atom's electric fields when passing close to a media atom. If these energy transfers do not exceed the electron binding energy (and therefore do not eject the electron), the atom is left in a disturbed / excited state.

Indirect Ionization – Gamma radiation (photons) passing through the media interact with the media atoms and form ion pairs through a photo ionization process, where the photon energy is transferred to the electron's kinetic energy. If this energy exceeds the electron binding energy, the electron is ejected (forming an ion pair). Photons possessing energies not sufficient to form ion pairs are either scattered or absorbed by the atom, leaving it in an excited state.

The number of ion pairs formed within the media is a function of the incident radiation's energy cross-section / spectrum and the nature of the media composition. In most substances, the energy lost in ion pair formation is larger than the ionization potential, which reflects the fact that some energy is lost in excitation.

5.1.2 Gas Filled Ion Chambers

The classical arrangement for an ion chamber is based on a hollow, sealed, gas filled (i.e., Xenon, Argon, etc.), conductive cylinder, typically having an aperture window of a selected material and a conductive filament positioned along the cylindrical axis, insulated from the cylinder's walls (Moore & Coplan, 1983). The dual electrode arrangement is formed by positively charging the filament (anode) and negatively charging the cylinder wall (cathode), through the application of a high voltage / potential (which produces an electric field within the chamber). Figure 5.1 provides a diagram showing the primary components of a gas filled ion chamber and the processes involved in its radiation detection / measurement process.

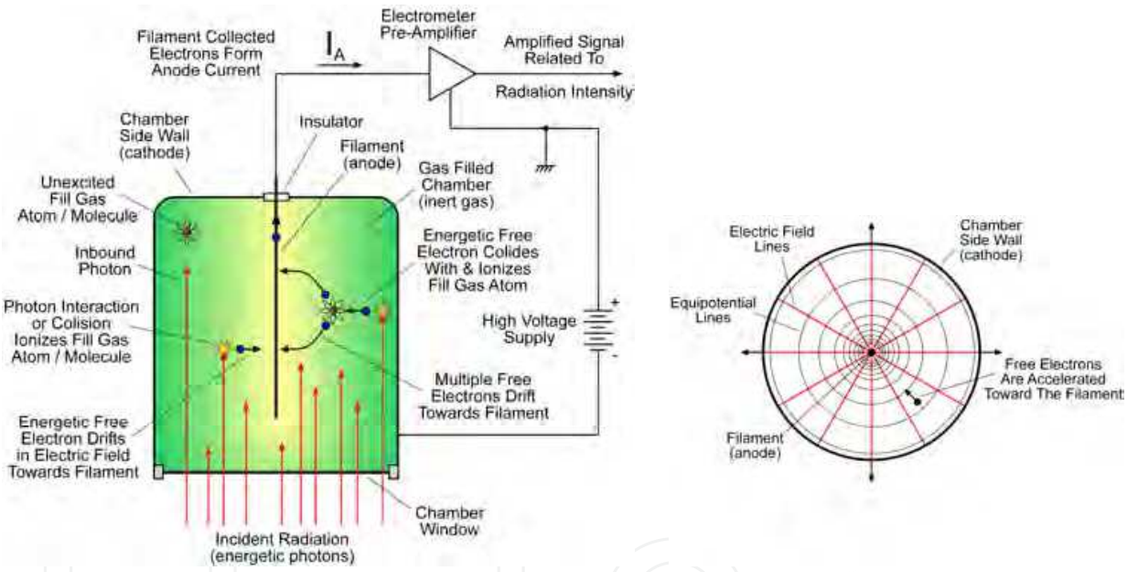

(a) (b)

Fig. 5.1 – Diagram showing the primary components of a gas filled ion chamber: a) Vertical cross-section view of the ion chamber components and processes involved in radiation detection / measurement, b) Cylindrical cross-section view showing the voltage applied electric field lines and associated equi-potential surfaces.

As radiation passes through the ion chamber's gas media, ion pairs are formed (by the processes mentioned above). The ionized gas atoms and free electrons drift and accelerate toward their respective electrodes. The speed (kinetic energy) at which these ion pairs migrate is a function of the chamber's electric field and composition / pressure of the media gas. The low mass of the free electrons causes them to move at much faster speeds toward the central filament.

The electrons (charge) collect on the anode filament, inducing a voltage change / current flow in the external circuitry connected to the anode, resulting in a pulse-like waveform. The amplitude of the pulse is dependent on the number of electrons collected by the filament. Although feeble (as low as tens of femto amperes), these currents can be detected and measured by electrometer class, transconductance amplifiers (Motchenbacher & Fitchen, 1973).

The amplitude of the filament current (for a given intensity of incident radiation) is a function of the applied chamber potential and the composition / pressure of the gas media (Moore & Coplan, 1983). Figure 5.2 provides a graphical description of filament pulse height as a function of chamber voltage.

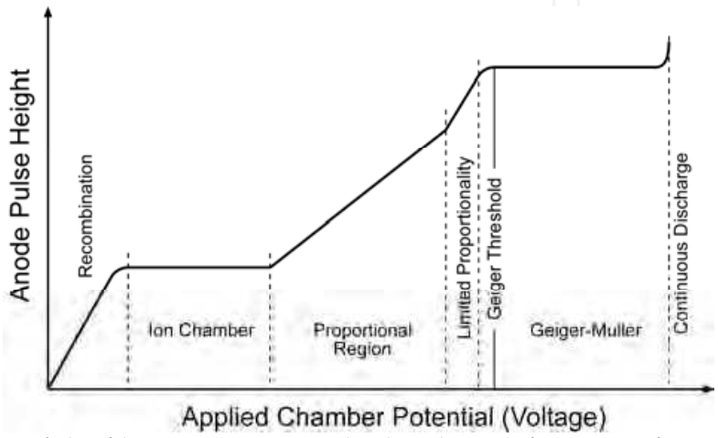

Fig. 5.2 – Behavior of the filament current pulse height as a function of applied potential, for a given constant intensity, incident radiation. This graph also shows the various regions of ion chamber operations.

Recombination Region – The chamber potential is relatively low, and the resulting electric field induced forces on the ion pairs (which draws them to the electrodes), is also low. The speed of electron drift toward the filament (anode) is slow, exposing some free electrons to high probabilities of being captured / neutralized by ions, before reaching the filament. Therefore, not all radiation induced ionization events are evidenced by the filament current. As the voltage is increased, the speed of drift also increases, and the probability of electron / ion neutralization diminishes, causing larger anode currents to be generated.

Ion Chamber Plateau – As the chamber potential is raised further, the rate of ion pair drift begins to reach speeds where the probability of neutralization (through recombination) is negligible. Essentially all of the free electrons formed by incident radiation ionization are collected at the filament. Here, the pulse amplitude levels-off, the anode current reaches a maximum value (for a given incident radiation level) and both no longer vary as functions of the applied voltage. This maximized filament current is often termed the saturation current, whose amplitude is dependent on the amount of received radiation. It is important to note that the formed free electrons gain energy as they drift and are accelerated by the electric field. In this voltage range, the electrons do not gain sufficient energy to induce subsequent ionization processes. If electron kinetic energies were to exceed the binding

energies of the gas atoms, then there would be an increase in the filament current, due to an effective increase in the gas amplification factor.

Proportional Region – With increasing chamber potential, the ion pair's kinetic energies are also increase (primarily noted by the speed of the free electrons). Here, these energies now exceed the gas atoms' binding energies, allowing the primary ions to generate secondary ions. This causes an amplification effect in the filament current. The electric fields are very concentrated local to the filament, and therefore the formation of secondary ions often occurs in the vicinity of the anode, and may induce additional orders of ion formation (essentially an avalanche behavior).

Geiger-Muller Plateau – As the chamber potential is raised further, electron drift speeds (kinetic energies) reach levels that generate photons as part of the secondary ionization processes. These emitted photons induce further ionizations to form throughout the entire chamber media. When operating in this region, it is not uncommon to augment the chamber's media with getter gasses (e.g., halogen) to provide a means of artificially quenching the high energy ion pairs, before secondary ionizations occur. When ion pairs encounter the getter gas molecules, they release certain levels of their energies to the molecules, then proceed with their drift trajectories at kinetic energies below the ionization potential of the base media. The resulting chamber behavior is highly responsive (fast), while also maintaining filament current proportional to the incident radiation intensity without a significant impact of secondary ionization effects.

Continuous Discharge – Beyond the Geiger-Muller region, the chamber potential reaches a level were the radiation induced ionization processes spontaneously erupts to form a sustained, non-dissipating plasma. The filament current can be significant (approaching the current limit of the high voltage power supply) and can damage sensitive external electronics / instrumentation. Under certain conditions, the chamber may experience "arching" discharges between the electrodes due to plasma associated changes in the media's dielectric properties.

5.2 Scintillation Based Detectors

Scintillation based detectors are a family of devices that employ a front-end sensor whose molecules have the property of luminescence (typically in the visible range) when exposed to ionizing radiation (Moore & Coplan, 1983). When incident radiation interacts with the sensor's molecules, the molecules absorb the inbound energy and enter an excited or ionized state. Upon neutralization or relaxation, the molecules emit a characteristics spectra associated with the recombinational spectral lines of the molecules / atoms. These fixed spectral emissions appear as momentary "flashes" of scintillating light (often in the visible range).

If the recombinational emissions occur immediately following the absorption of the inbound radiation energy (< 10 pico seconds), the resulting luminescence process is termed fluorescence. If the recombination / relaxation occurs following a discernable delay, the process is termed phosphorescence or after-glow.

The front-end scintillation sensor is typically composed of a inorganic compounds (e.g., Sodium Iodide, Bismuth Germanate) or an organic fluid, having high quantum efficiencies.

The quantum efficiency is associated with the density of electrons in the compound's molecules / atoms, generally due to high atomic number of the elemental constiuents. Perhaps the most widely used scintillation compound is Sodium Iodide activated with metal ions in Thallium, NaI(Tl).

5.2.1 Scintillation Crystal / Photomultiplier Tube

A classical scintillation based detector involves the pairing of a Sodium Iodide crystal with a photomultiplier tube (PMT) (Moore & Coplan, 1983), (RCA, 1963). Figure 5.3 provides an illustration of this arrangement, the primary components.

Radiation incident to the Sodium Iodide crystal induces a scintillation luminance in the form of characteristic, recombinational spectral emissions, with intensities proportional to the intensity of the inbound radiation. This scintillated light is transmitted-to and strikes the PMTs photocathode, forming free electrons as a consequence of the photoelectric effect.

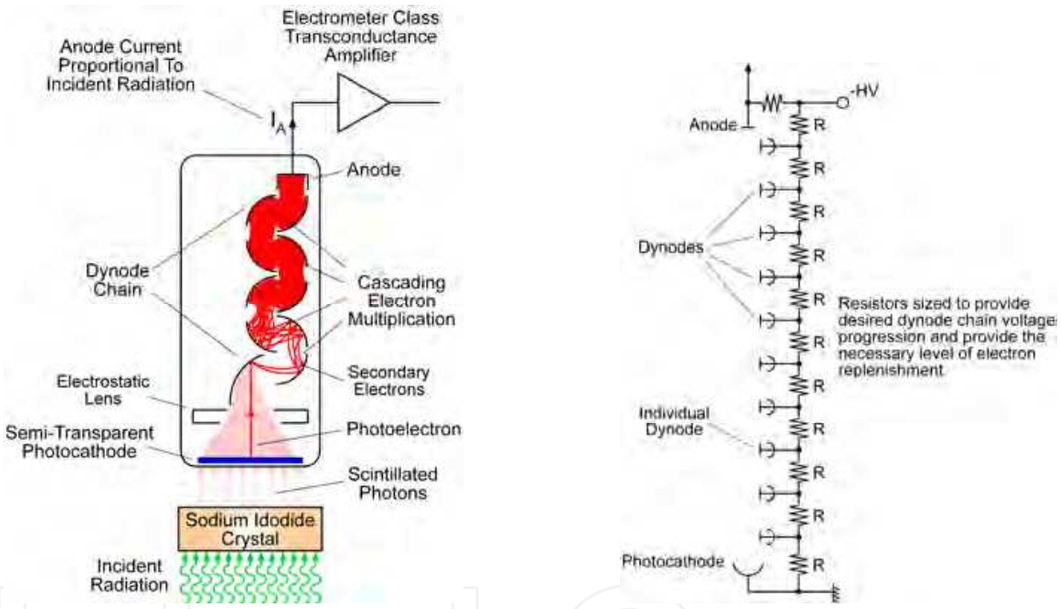

(a) (b)

Fig. 5.3 – Diagram showing the primary components of a scintillation detector based on a Sodium Iodide crystal paired with a photomultiplier tube: a) Primary components and illustration of the electron multiplying effect, b) Electrical schematic of the PMTs dinode chain.

The photoelectrons depart the photocathode with a kinetic energy related to the energy of the incoming photon (reduced by the losses of the work function of the photocathode). The PMTs photocathode and electron multiplying dynode chain are charged with progressively more positive voltages, generating an electric field that draws and accelerates the free electrons from the photocathode, to the dynode chain. An electrostatic lens group is often employed to focus / direct the photoelectrons onto the surface of the first dynode.

The accelerated photoelectrons impact the first dynode (at a relatively high energy), and release a group of lower energy electrons (by the process of secondary emission). This group of lower energy electrons are accelerated towards the next dynode, where their increased kinetic energy, releases more electrons (an electron multiplication effect). The organization of the dynode chain causes a cascading / ever-increasing number of electrons to be produced at each stage. The multi-stage / multiplied electrons reach the anode (final stage) with a large charge accumulation, which results in a large current pulse that is directly related to an arrival event of a scintillation photon at the photocathode.

The anode current can be collected and assessed in several ways. For ultra-low radiation intensities (i.e., < 1000 events per second), the individual photon encounter event is directly related to an anode current pulse. Pulse discrimination and counting methods can be applied to measure the broad spectrum radiation intensity. Alternatively, pulse height and height distribution analysis can be employed to measure the radiation cross-section. Typically, the radiation source and measurement system are designed to induce a sufficiently large intensity of inbound radiation, that the resulting anode waveform is a near continuous current. Here, electrometer class, transconductance amplifiers (Motchenbacher & Fitchen, 1973) are applied to create usable signal levels in subsequent signal processing stages.

6. Rendering a Thickness Measurement

The primary function of the systems under consideration, is to render a measurement of the material thickness. Fundamentally, this involves the rearrangement of the complex relationship of Eq(5.1), to isolate "x", the material thickness. This is a non-trivial exercise and is not well suited for this level of discussion. However, it is possible to examine the simplified case for monochromatic incident radiation. Returning to Eq(4.3), and assuming the detector signal, I_D, is directly related to the transmitted radiation intensity, we have:

$$I_D \sim I_0 e^{-\left(\frac{\mu}{\rho}\right)\rho x} = I_0 e^{-\frac{x}{q}} \tag{6.1}$$

Isolating the material thickness, x, and considering the calculated value to be an "estimate" of the thickness, $\hat{x}$, based on the available knowledge of the alloy and generated radiation, I_0, results in:

$$X_M = \hat{x} \sim -\left(\frac{\rho}{\mu}\right)\frac{1}{\rho}\ln\left[\frac{I_D}{I_0}\right] = q\left(\ln(I_0) - \ln(I_D)\right) \tag{6.2}$$

The rendered thickness measurement, X_M, is the final indication of the absolute thickness, expressed in a chosen engineering unit of measure. Perhaps the most daunting issue that confronts rendering the thickness measurement, is having sufficient knowledge of the alloy or constituents that form the material, and make-up the Mass Attenuation Coefficient (MAC) energy cross-section. Minor variations in the understood versus the actual MAC can have dramatic effects on the quality / accuracy of the measurement.

6.1 Signal Processing and Data Flow

The digital signal processing sequence that is typically involved in rendering the thickness measurement is shown in Figure 6.1.

Front-End Analog Signals – The detector signal is amplified by an electrometer class pre-amplifier. It is important that this signal set be carefully shielded to prevent interference from external electrostatic noise sources. Often, the detector and pre-amplifier are located within the same shielded housing. The pre-amplifier is band-limited to provide a degree of noise suppression without compromising the temporal dynamics of the material under examination (often the material is in a transport condition with speeds up to 1500 meters / minute, and it is necessary to be able to accurately track thickness variations evolving over 50mm segments (2 millisecond period – 1000Hz minimum Nyquist BW).

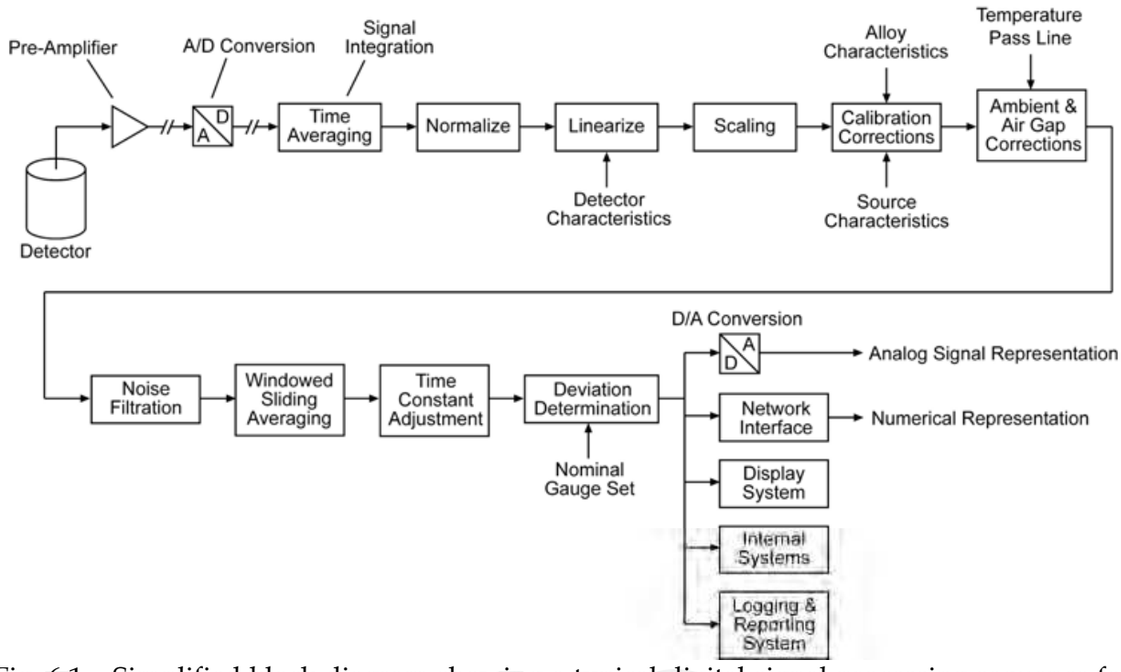

Fig. 6.1 – Simplified block diagram showing a typical digital signal processing sequence for thickness rendering and the transmission of the measurement signal to other systems.

Analog / Digital Conversion (A/D) – The analog pre-amplifier signal is digitized to a numerical form with high resolution (16 bits or greater). It is desirable that this conversion be performed as close as possible to the pre-amplifier to minimize signal runs (length) and the influence of external noise sources on the analog measurement signal. It is not uncommon to locate the A/D converter in close proximity to the detector / pre-amplifier housing (thereby minimizing analog signal runs). The digital / numerical representation of the measurement signal can then be transmitted large distances via noise immune techniques. Typical sampling periods are on the order of 250 microseconds, however slower or faster rates are well within the capabilities of the electronics, and primarily application dependent.

Signal Integration – The numerical measurement signal is integrated over a fixed time interval (typically through simple averaging or low pass filtering methods) to maximize the signal to noise ratio, prior to further signal processing (Bose, 1985). The bandwidth / windowing characteristics of this stage must be selected to not impact the bandwidth of the measurement of the fundamental process (actual material thickness temporal variations).

Normalization – To maximize the signal's dynamic range, the integrated signal can be optionally normalized to a standard signal level framework (often associated with the numerical representation of subsequent signal processing components).

Linearization – Any non-linear aspects of the detector's response characteristics are removed to provide a well defined linear relationship between the measured radiation intensity and the numerical measurement signal.

Scaling – The numerical measurement signal is be converted to engineering / radiometry units from which calibrated adjustments and standardized material / radiation characteristics can be applied.

Calibrated Corrections – This signal processing component often involves the most complex mathematics and numerical methods. The characteristics of the material composition and the radiation source are considered in rendering an initial assessment of the material thickness.

Ambient & Air Gap Corrections – The initial thickness measurement is adjusted to correct for ambient conditions (primarily the air gap temperature and the material temperature) and for known variation in the pass-line. The output signal from this stage is the fundamental thickness measurement. Any subsequent processing of this signal is associated with application specific requirements and compensations.

Noise Filtration – This optional, switchable, programmable filtering stage is applied to situations where expected or unavoidable process related conditions may increase the uncertainties in the measurement accuracy. The nature and operation of this filtration is purely situation dependent and can be as simple as a reduction in the measurement bandwidth, to a sophisticated multi-variable compensation specific to a characterizable disturbance (e.g., uncertainties due to pass-line variations associated with the vertical displacement of vibrating strip), (Bose, 1985).

Windowed Sliding Averaging – This optional signal processing is applied to provide a specific waveform shaping of the measurement signal. This can be employed to assist downstream / related control equipment in compensating for certain process dynamics, (Bose, 1985).

Time Constant Adjustment – To external equipment / observers, the overall measurement system provides an estimate of the material thickness having a programmable, specifiable bandwidth and / or first-order, step function response. Although the fundamental measurement signal may have a relatively wide bandwidth, external equipment may have lower bandwidth input and / or anti-aliasing requirements. This final stage of filtering provides and output signal that corresponds to the bandwith / step function time constant requirement of the external equipment.

Deviation Determination – The rendered signal, X_M, provides an indication of the absolute material thickness, X. External equipment (e.g., Automatic Gauge Control (AGC) systems, Statisical Process Control (SPC) recorders, etc.) may require the measurement system output signal in terms of the Deviation, ΔX_M, about a Nominal Set Thickness, X_{Nom}.

Signal Distribution – The final measurement signal is provided to external equipment via a variety of means. Analog signal representations can be generated to support legacy class systems. Networked interface can provide fully numerical measurement and status data. Display systems ranging from simple metering to sophisticated Graphical User Interface (GUIs) and visualization can be provided to human operators. The measurement system can also provide a variety of internal function based on the final measurement signal (including FFTs, SPC, performance monitoring, status reporting, etc.).

6.2 Characterizing the Measurement Signal

The rendered measurement signal can be transmitted and provided over a number of media and a broad range of formats. At their root, at the completion of the measurement process, the instrument forms a final determination of the material thickness, X_M.

This measurement signal is an indication of absolute thickness, expressed in a chosen engineering unit of measure. The measurement value resides in an internal memory register (possibly fixed or floating point). The value is presented in a number of significant digits, functionally related to the instrument's finest resolution. The signal will operate as a discrete time numeric and be updated at a high frequency.

6.2.1 Signal Formats

There are two(2) primary formats involved in measurement signal transmissions and displays (both graphical and numerical):

Actual Value – This involves the direct transmission of the unipolar material thickness measurement, X_M, in either absolute engineering units or as a percent of Full Scale Range (FSR). When considering analog signals, this format is often expressed in terms of thickness per volt (0.50 mm/volt for a 5mm FSR on a 0-10 volt output range) or percent per volt (0-10 volts equals 0-100% of the FSR). This programmable scaling factor can be adjusted to suit the application of the receiving equipment.

Deviation Value – This involves the transmission of a bipolar deviation signal, ΔX_M, about a nominal thickness value, X_{Nom}, and is provided in either engineering units or a percent of the deviation range. The sum of these signals being the actual thickness value, X_M. The deviation signal is developed as follows:

$$\Delta X_M = X_M - X_{Nom} \tag{6.3}$$

The nominal thickness is typically provided as an operating set-point issued by the end-user / operator or by an overseeing automation system. This arrangement is often preferred when providing thickness readings to thickness control systems (AGC) or quality control / tracking systems (SPC), since the signal accuracy and resolution can be greatly increased. When considering analog signals, this format is often expressed in

terms of thickness per volt (25 μm/volt for a +/-0.250mm FSR on a +/-10 volt output range) or percent per volt (+/-10 volts equals +/-100% of the deviation's FSR). This programmable scaling factor can be adjusted to suit the application of the receiving equipment.

6.2.2 Time Response Characterization

The temporal behavior / performance of the measurement signal is classically characterized in terms of a 1st order step response, with the time constant being the key indication of merit. Typical time constants range from 5-200 milliseconds, depending on the accuracy and dynamic response requirements of the application. Most high performance cold rolling and strip processing applications involve time constants on the order of 5-20 milliseconds. Figure 6.2 provides a graphical representation of the time evolution of a classical 1st order step response.

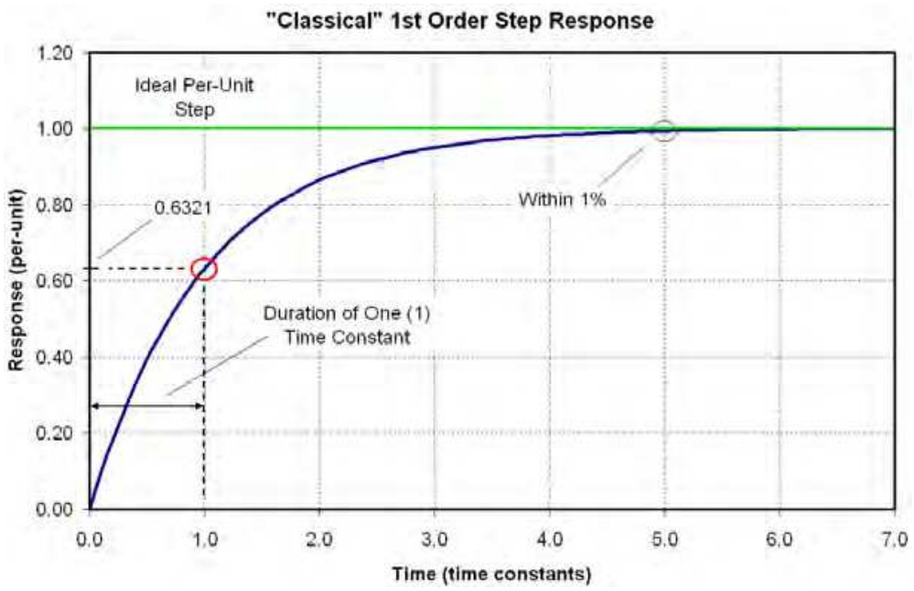

Fig. 6.2 – "Classical" 1st Order Step Response and associated parameters.

The factors (from Figure 6.1) that contribute to the time constant are:

- Pre-Amplifier Band-Limiting Filtration
- Signal Integration / Time Averaging
- Specific Noise Filtration
- Windowed Averaging
- Direct Time Constant Filtration
- Application's Dynamic Response Requirements
- Application's Noise Level and Accuracy Requirements

Realistically, the actual gauging system time response characteristic are more complex and tend to contain higher order dynamics introduced by the signal processing and filtration activities. Specific characterizations of the time response are provided in international standards (IEC, 1996).

Regardless of the signal amplitude resolution, the temporal resolution of the signal's updates plays a key role in the quality and apparent continuity of the provided measurements. Figure 6.3 provides a graphical comparison of the signal fidelity for different signal update rates.

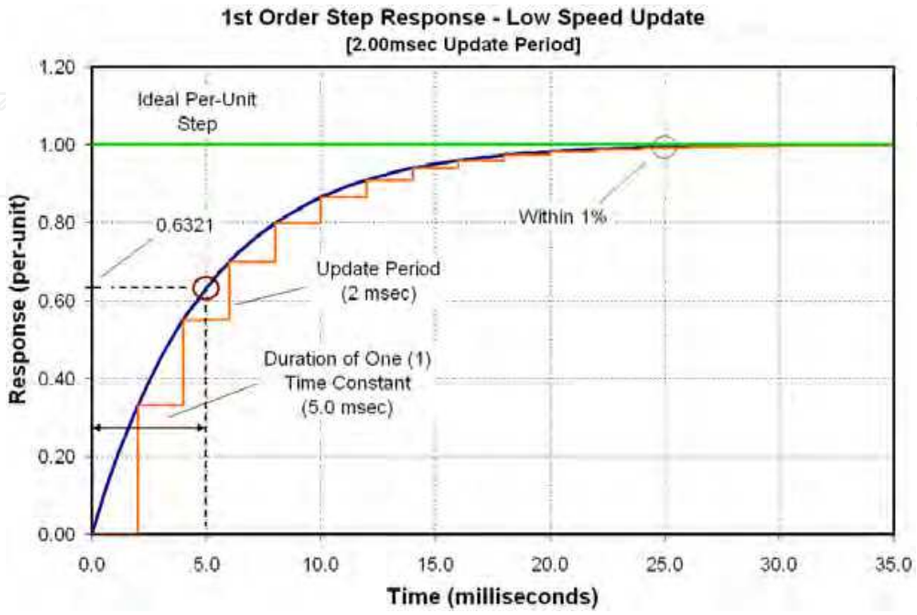

(a)

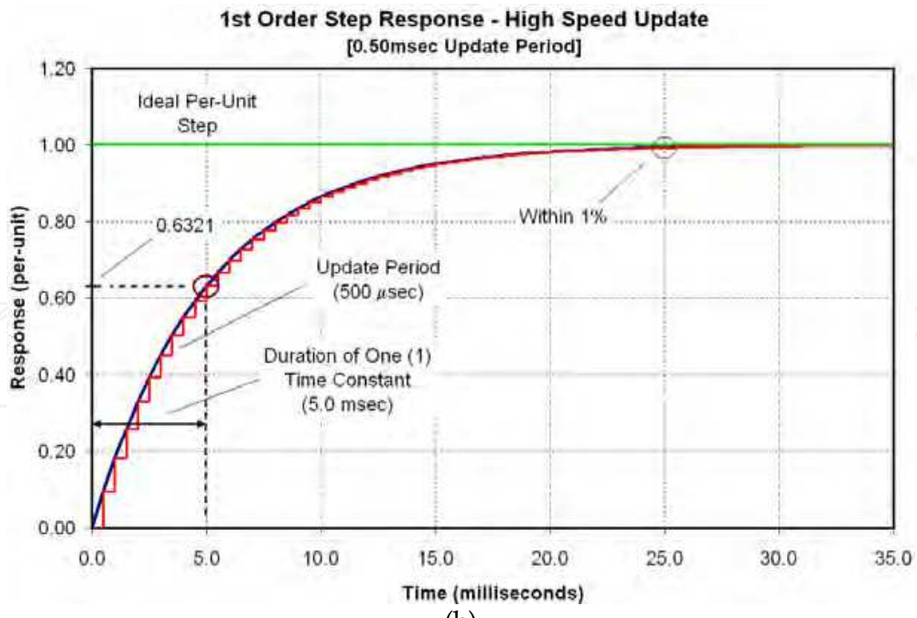

(b)

Fig. 6.3 – Comparison of the influence of update rates on the "fidelity" of the measurement signal having a 5.0 millisecond time constant: a) Time response involving a 2.00 millisecond update period, b) Time response involving a 0.50 millisecond update period.

Beyond the rather crude and abrupt behavior of the slower update signal (see Figure 6.3a), this behavior also introduces a notable phase lag. Downstream systems may require a knowledge of this phase lag to take the necessary compensating actions.

It is possible to further extend the evaluation of the specific time response characteristics to more realistic strip processing through spatial wavefront analysis (I2S, 2004), to account for the passage of abrupt or non-uniform thickness variations through the fast moving strip's beam intercept area (typically circular with a 25mm diameter). However, these subjects are beyond the scope of this discussion.

6.2.3 Measurement Performance Indicators

Accuracy, precision, resolution, repeatability and reproducibility are key terms in specifically describing the fundamental measurement characteristics of the instrument. There are many good sources defining and describing the various aspects of measurement performance (Cooper, 1978) (IEC, 1996) (Nyce, 2004). For the purposes of these discussions, we will concern ourselves with only certain fundamental indicators.

Accuracy – The degree of conformity of a measured or indicated quantity to the actual (true) value. This performance measure is typically expressed as a combination of relative uncertainty and / or absolute uncertainty, in terms of a standardized engineering unit.

> Accuracy : +/-0.1% of the nominal thickness or +/-0.50μm, which every is greater, with all alloy compositions resolved and calibrated.

This indication can be based on a statistical sense (2σ – 95.4% of readings) or as a bounding, worst case condition.

Precision – A measure of the degree to which successive measurements differ from one another, over a certain time interval (typically minutes), given the same condition and operating in the same environment. Precision is typically expressed as a combination of relative uncertainty and / or absolute uncertainty, about a nominal operating point, in terms of a standardized engineering unit.

> Precision : +/-0.1% of the nominal thickness or +/-0.50μm, which every is greater, in a statistical sense (2σ – 95.4% of readings)

This is often described in terms of a statistical noise envelope of uncertainty associated with any measurement, and the specifications may include an admissible time interval between the measurements and the last standardization.

The definitions of accuracy and precision are often a point of unnecessary confusion and conflict. Figure 6.4 provides an illustration of typical time evolution and amplitude distribution of a thickness deviation signal. Figure 6.5 provides a simple depiction of accuracy and precision when the measurement system's, instantaneous uncertainty characteristics. Figure 6.6 extends these concepts to illustrate the implications of the various combinations of good and bad, accuracy and precision. When formulating or assessing these measures of performance, it is important to grasp the specifics and relevance of their indications with respect to the application requirements.

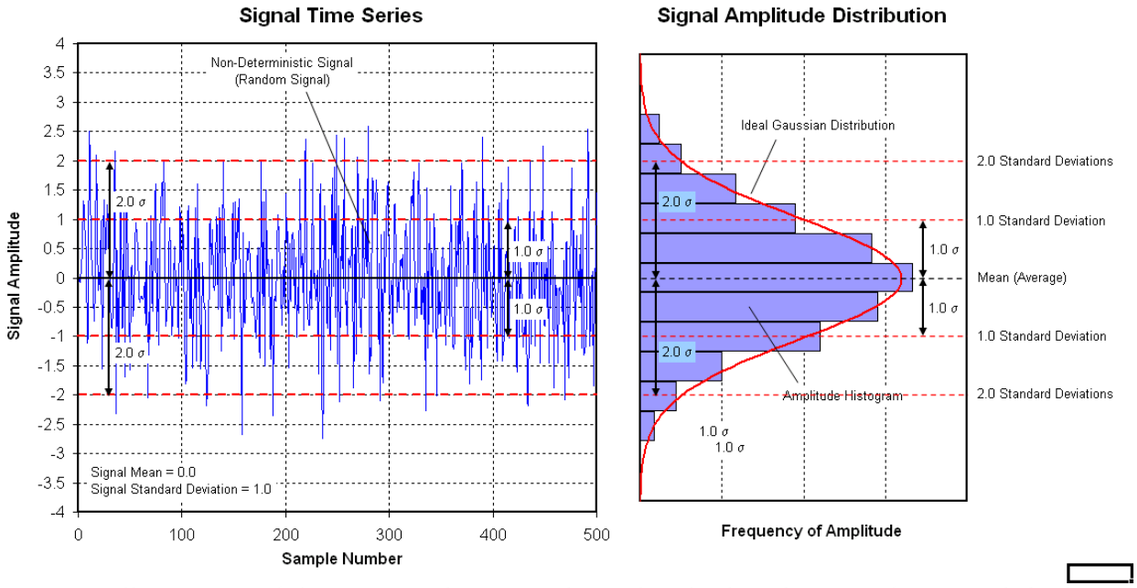

Fig. 6.4 – Illustration of the time evolution and amplitude distribution of a typical thickness measurement deviation signal.

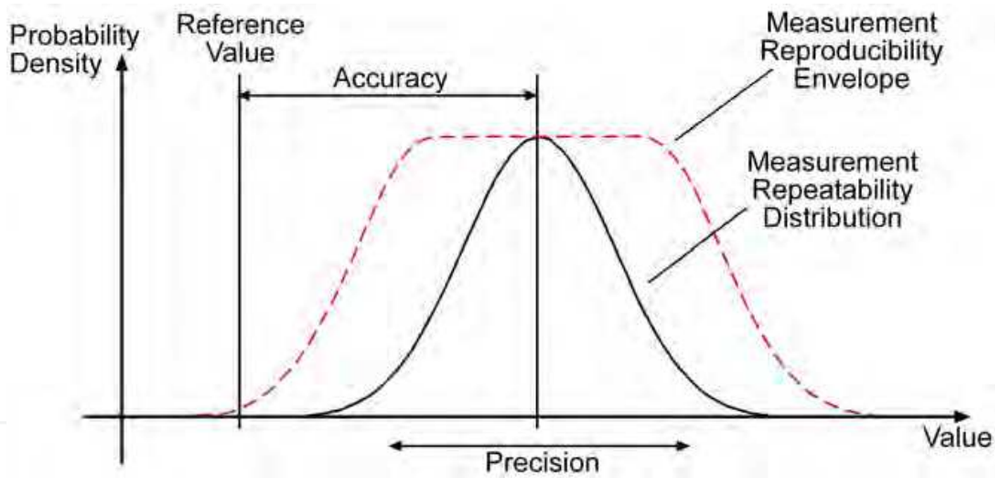

Fig. 6.5 – Fundamental definition and concepts of accuracy and precision, when the measurement uncertainties can be characterized as a white noise having Gaussian amplitude distribution.

Continuing with the definitions:

Repeatability – The closeness of agreement among the results of a number of successive measurements taken for the same value of input under the same operating conditions, over a specific interval of time (often minutes). The standard deviation, σ, of the set of repeatability measurements (often the 2σ indication) is typically used as a measure of precision (see above).

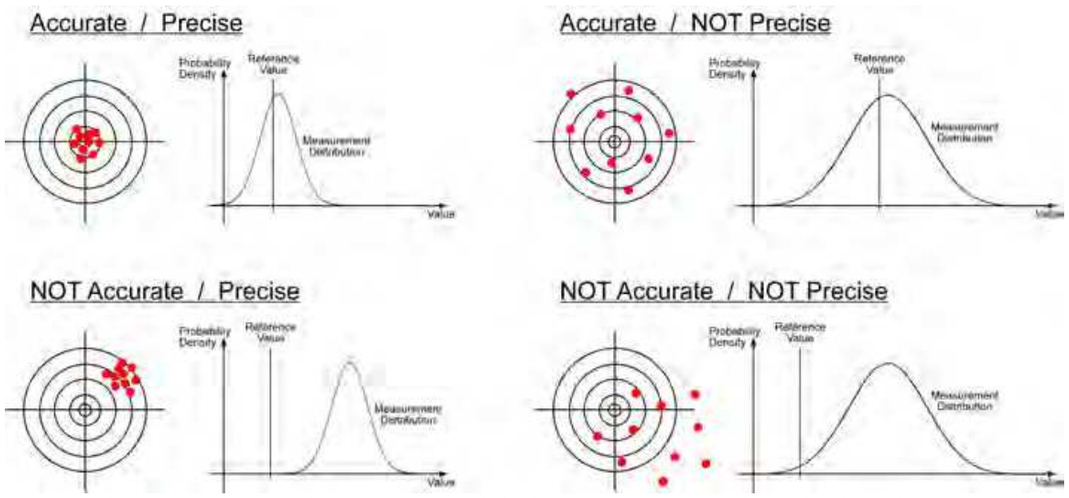

Fig. 6.6 – Comparison of the nature and behavior associated with data having differing levels of accuracy and precision.

Reproducibility – The closeness of agreement among the results of a number of successive measurements taken on the same instrument for the same value of input under the same operating conditions, over an extended interval of time (often hours or days). This means the degree to which a measurement can be replicated independently. This term can be extended to include multiple independent instruments (possibly of the same model or method), to characterize the similarity of measurement s taken (by a product line). Essentially, reproducibility is a bounding envelope, constraining the variability of the accuracy and precision of the instrument, over extended time intervals (see Figure 6.5). Therefore, the instrument's reproducibility is subject to influences of accuracy and precision / noise issues. Reproducibility is typically expressed as a relative or absolute variability bounds and may be based on the standard deviation (often the 2σ indication) of the set of measurements taken over extended periods of time, or a worst case bounding condition.

Reproducibility: +/-0.05% of the nominal thickness or +/-0.25μm, which every is greater, with all alloy compositions resolved and calibrated.

It can also be applied as a permissible range of variability of the mean of the set of repeatability measurement groups taken over long periods of time or on different / independent instruments.

Drift – This describes the variance of the mean of a set of successive groups over a period of time, and serves as a measure of instrument stability. Drift is typically expressed as a relative or absolute variability bound, often as a worst case bounding condition over an interval of time.

Drift : +/-0.1% of the nominal thickness over an 8 hour period

Drift variances are usually determined from an assessment of the mean of repeatability measurements taken at specified intervals of time, and evaluated for long term trending behaviour.

Resolution – The smallest change of the quantity being measured to which the instrument will respond and a change in the measurement signal can be observed or detected. Instrument resolution is related to the precision at which the measurement was made and to the Minimum Detectable Signal (Motchenbacher & Fitchen, 1973) which is typically defined as twice the system noise level (precision). Resolution can also be defined in terms of the quantization or significant digits of the numerical representation (i.e., 16 bit resolution or 6 significant digit display) over a specific operating range. This infers a Least Significant Bit (LSB) / single digit quantization, which may be misleading and have no relationship to the actual instrumentation resolution. Resolution differs from quantization, in that quantization is a mapping process from a continuous range of values to a discrete set of values having a minimum quanta (LSB).

Linearity – This closeness that the calibrated, standardized instrument approximates a straight line response over a specified measurement range. Linearity is typically expressed as an absolute or relative indication of the maximum differences between the instrument's readings and the actual values, over a measurement interval.

Linearity : +/-0.1% of the FSR over a +/-1.0 mm range from the standardized nominal thickness

Some instruments operate in a narrowly defined region of the overall range of measurement capabilities. Here, linearity also provides an indication of the breadth of the localized measurement range, before a distortion appears on the instrument's output.

7. System Sensitivity Characteristics and Relationships

When assessing a measurement produced by these forms of instruments, we must be cognizant of the many influences that can distort or corrupt the accuracy or quality of the measurement.

7.1 General Sensitivity

For a constant incident radiation intensity of, I_0, the general sensitivity is defined as the relative variations in emitted beam intensity, I, corresponding to the relative variations in the material thickness, x.

$$S = \frac{\frac{dI}{I}}{\frac{dx}{x}} \tag{7.1}$$

From Eq(4.1) we have:

$$dx = -\left(\frac{\rho}{\mu}\right)\frac{1}{\rho}\frac{dI}{I} = -\frac{1}{\mu}\frac{dI}{I} = -q\frac{dI}{I} \tag{7.2}$$

Resulting in:

$$S = -\left(\frac{\mu}{\rho}\right)\rho x = -\mu x = -\frac{x}{q} \tag{7.3}$$

In making S as large as possible, we see that there are two(2) possible degrees of freedom.

- Increasing the attenuation by operating at lower energy levels
- Operating at the maximum thickness the instrument can measure.

In practice, the choice of the thickness range and the operating energy is based on the application and instrument characteristics.

7.2 Statistical Noise

The random behavior of the atomic transformation process (fundamentally Poisson statistics) and the random nature of X-Ray photon emissions from electron beam formation and bombardment (primarily a function of micro fluctuations in filament temperature and current, like a shot noise) can be characterized as a zero mean, white noise superimposed on the measured signal. The standard deviation of a monochromatic noise function, when measured over a given integration time, $\Delta\tau$, can be characterized by : (Motchenbacher & Fitchen, 1973)

$$\frac{\sigma(I)}{I} = \frac{K}{\sqrt{\Delta\tau \cdot I}} \tag{7.4a}$$

$$\sigma(I) = K\sqrt{\frac{I}{\Delta\tau}} \tag{7.4b}$$

where K is a constant. When considering the effect of this noise on the measurement signal, $\hat{x}$, can be obtained from combining Eq(7.1) and Eq(7.3)

$$\frac{\partial x}{x} = -\left(\frac{\rho}{\mu}\right)\frac{1}{\rho x}\frac{\partial I}{I} = \frac{-1}{\mu x}\frac{\partial I}{I} = -\frac{q}{x}\frac{\partial I}{I} \tag{7.5}$$

As a consequence, the relative statistical variation in the measured thickness can be provided by:

$$\frac{\Delta x}{x} = -\left(\frac{\rho}{\mu}\right)\frac{1}{\rho x}\frac{K}{\sqrt{\Delta\tau \cdot I}} = \frac{-1}{\mu x}\frac{K}{\sqrt{\Delta\tau \cdot I}} = -\frac{q}{x}\frac{K}{\sqrt{\Delta\tau \cdot I}} \tag{7.6}$$

Combining Eq(6.1)

$$\frac{\Delta x}{x} = -\left(\frac{\rho}{\mu}\right)\frac{1}{\rho x}\frac{K \cdot e^{\frac{1}{2}\left(\frac{\mu}{\rho}\right)\rho x}}{\sqrt{\Delta\tau \cdot I_0}} = \frac{-1}{\mu x}\frac{K \cdot e^{\frac{1}{2}\mu x}}{\sqrt{\Delta\tau \cdot I_0}} = -\frac{q}{x}\frac{K \cdot e^{\frac{1}{2}\frac{x}{q}}}{\sqrt{\Delta\tau \cdot I_0}} \tag{7.7}$$

Figure 7.1 provides a graphical comparison of the relative statistical measurement noise for various integration time intervals. The important aspects of this figure are the integration time independent, noise minimum at the optimal thickness of:

$$x_{Opt} = 2q \tag{7.8}$$

Noise associated with shorter Mean Free Paths have reciprocal behavior, while longer paths have exponential characteristics. Also important is the elevation of the noise function as a function of the reciprocal of the square root of the integration interval.

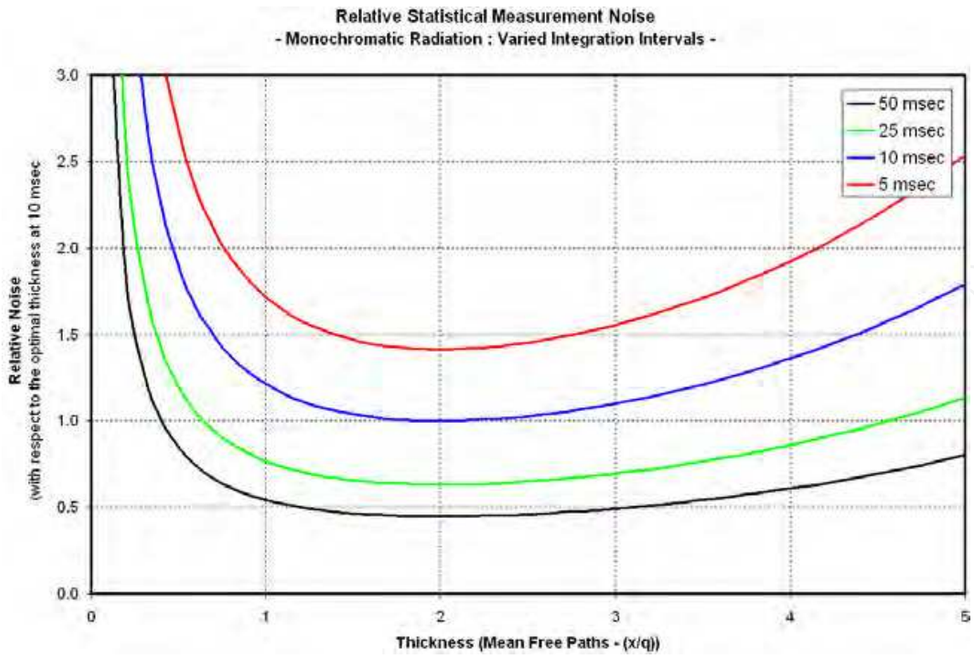

Fig. 7.1 – Comparison of the relative statistical measurement noise for monochromatic radiation as a function of the Mean Free Paths of thickness, for various integration times.

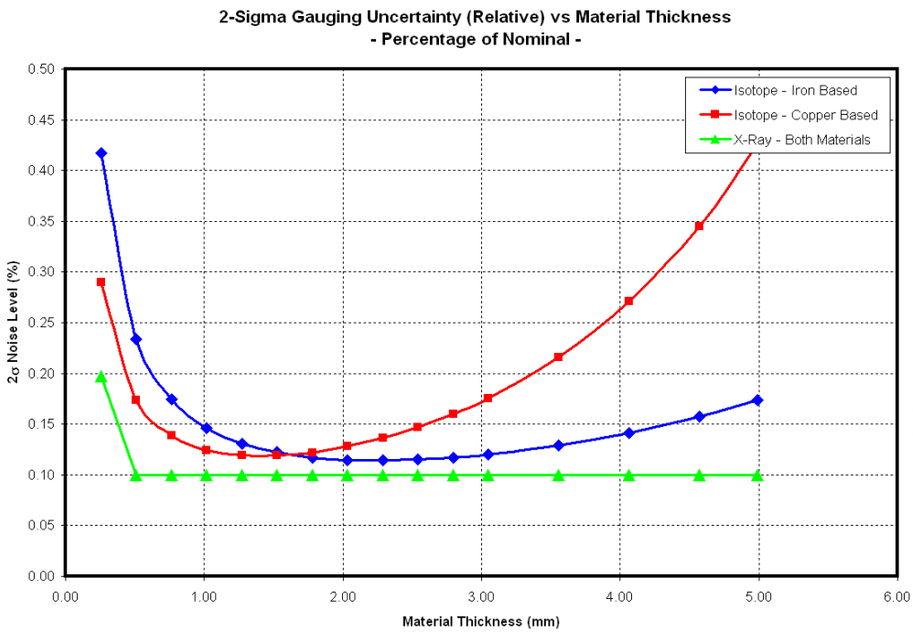

Fig. 7.2 – Comparative plot of the actual noise functions (2σ of the nominal thickness) of a monochromatic 1.0 Ci Americium 241 source applied to NIST Traceable samples of know steel and copper alloys, for a 25 msec integration period. This plot includes the noise function of an X-Ray based instrument (operating with a 10 msec integration period) employing tube potential adjustment to maintain a constant signal-to-noise ratio for thicknesses above 0.5μm.

The relationships of Eqs(7.4) through Eq(7.8) are associated with monochromatic radiation, and therefore are suitable for characterizing isotope sources (e.g., Americium 241). Figure 7.2 provides some instrument performance data for a 1.0 Ci Americium 241 source, applied to NIST Traceable samples of known steel and copper alloys.

This comparative plot shows the variations in the optimal thickness as a function of material composition. This plot also includes the noise function of an X-Ray based instrument employing tube potential adjustment to maintain a constant signal-to-noise ratio. In this case, the choice of applied tube voltage is focused on optimizing the noise level while simultaneously maintain a specific level of signal sensitivity. Further, the X-Ray system is operating with a 10 msec integration period, and achieving better performance. This is primarily because of the degrees of freedom available to the X-Ray gauge's operating point (beam current, tube potential, filament current stability, etc.).

When considering the polychromatic radiation of the X-Ray generator, it's necessary to consider the energy dependencies of the source's applied radiation and the material.

$$\frac{\Delta x}{x}(\lambda) = -\left(\frac{\rho}{\mu}(\lambda)\right)\frac{1}{\rho x}\frac{K\cdot e^{\frac{1}{2}\left(\frac{\mu}{\rho}(\lambda)\right)\rho x}}{\sqrt{\Delta\tau\cdot I_0}} = \frac{-1}{\mu(\lambda)x}\frac{K\cdot e^{\frac{1}{2}\mu(\lambda)x}}{\sqrt{\Delta\tau\cdot I_0}} = -\frac{q(\lambda)}{x}\frac{K\cdot e^{\frac{1}{2}\frac{x}{q(\lambda)}}}{\sqrt{\Delta\tau\cdot I_0}} \qquad (7.9)$$

This non-trivial expression is typically not analytically evaluated to determine the optimal noise level, but is often found through empirical characterizations with standardized samples and calibration procedures (Howard, 1970).

It is also possible to express the measurement noise in terms of an absolute thickness variation. Returning to Eq(7.7), statistical noise expressed in terms of absolute thickness is:

$$\Delta x = -\left(\frac{\rho}{\mu}\right)\frac{1}{\rho}\frac{K\cdot e^{\frac{1}{2}\left(\frac{\mu}{\rho}\right)\rho x}}{\sqrt{\Delta\tau\cdot I_0}} = \frac{-1}{\mu}\frac{K\cdot e^{\frac{1}{2}\mu x}}{\sqrt{\Delta\tau\cdot I_0}} = -q\frac{K\cdot e^{\frac{1}{2}\frac{x}{q}}}{\sqrt{\Delta\tau\cdot I_0}} \qquad (7.10)$$

This function's behavior is largely exponential with a minimum at zero thickness (i.e., solely a function of the statistical variations of the source's radiation, I_0, and the integration period. Figure 7.3 provides the associated instrument performance data of Figure 7.2, in absolute terms.

7.3 Sensitivity to X-Ray Tube Voltage Variations

As shown in Figure 3.9, the X-Ray Tube's emitted intensity, I_0, varies with the applied potential (tube voltage), V_X. For the range of interest, the relationship between the intensity and applied voltage can be given by:

$$I_0 \sim K_V\left(V_X\right)^3 \qquad (7.11)$$

and the MAC behavior (in the 10kV to 100kV range – primarily Photoelectric Absorption) can be described with:

$$\frac{\mu}{\rho} \sim \frac{K_{MAC}}{\rho\cdot\left(V_X\right)^3} \;\Rightarrow\; q = K_{MAC}\left(V_X\right)^3 \qquad (7.12)$$

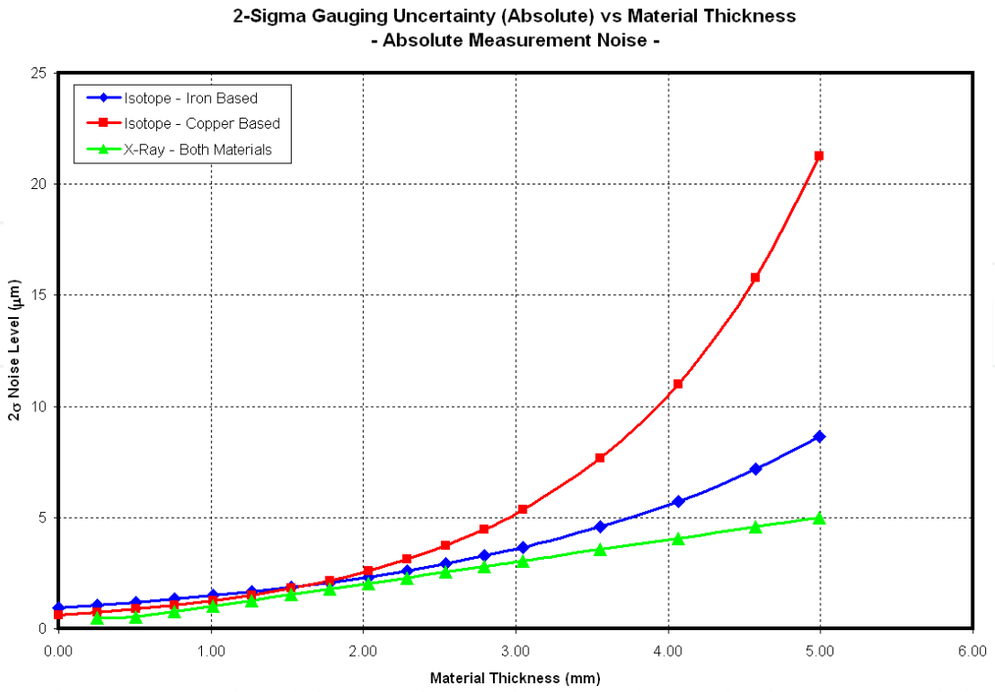

Fig. 7.3 – Comparative plot of the actual noise functions (2σ in absolute measured thickness variations) based on the instruments and situations associated with Figure 7.2.

where K_V and K_{MAC} are instrument dependent constants. From Eq(4.2) we have:

$$\ln(I) = \ln(I_0) - \left(\frac{\mu}{\rho}\right)\rho x = \ln(I_0) - \frac{x}{q} \tag{7.13}$$

Substituting Eqs(7.11, 7.12) results in:

$$\ln(I) = \ln\left(K_V (V_X)^3\right) - \frac{x}{K_{MAC}(V_X)^3} = \ln(K_V) + 3\ln(V_X) - \frac{x}{K_{MAC}}(V_X)^{-3} \tag{7.14}$$

Continuing and differentiating with respect to V_X provides:

$$\frac{\partial(\ln(I))}{\partial V_X} = \frac{1}{I}\frac{\partial I}{\partial V_X} = \frac{3}{V_X} + 3\frac{x}{K_{MAC}}(V_X)^{-4} = \frac{3}{V_X} + 3\frac{x}{K_{MAC}}\frac{(V_X)^{-3}}{V_X} \tag{7.15a}$$

or with Eq(7.12)

$$\frac{\partial I}{I} = 3\frac{\partial V_X}{V_X} + 3\frac{x(V_X)^{-3}}{K_{MAC}}\frac{\partial V_X}{V_X} = 3\left(1 + \left(\frac{\mu}{\rho}\right)\rho x\right)\frac{\partial V_X}{V_X} = 3\left(1 + \frac{x}{q}\right)\frac{\partial V_X}{V_X} \tag{7.15b}$$

Returning to the fundamental sensitivity relationship of Eq(7.2), we have:

$$\frac{\partial I}{I} = -\mu\,\partial x = -\frac{\partial x}{q} \tag{7.16}$$

Introducing this into Eq(7.15b) results in:

$$\partial x = -\frac{3}{\rho}\left(\frac{\rho}{\mu}\right)\left(1+\left(\frac{\mu}{\rho}\right)\rho x\right)\frac{\partial V_X}{V_X} = -3q\left(1+\frac{x}{q}\right)\frac{\partial V_X}{V_X} \tag{7.17}$$

The corresponding relative variations in the measured thickness associated with relative variations in the applied tube voltage are:

$$\frac{\Delta x}{x} = -3\left(\left(\frac{\rho}{\mu}\right)\frac{1}{\rho x}+1\right)\frac{\Delta V_X}{V_X} = -3\left(\frac{q}{x}+1\right)\frac{\Delta V_X}{V_X} \tag{7.18}$$

This is an important relationship, because it defines the impact of the applied voltage regulation quality on the measurement signal. Because of its relative use of the applied voltage, the relationship is a reciprocal function is MAC / MFP, and always acts as an amplification factor (asymptotically approaching its minima of -3). This requires exceedingly good voltage regulation, especially for thicknesses below an MFP of 1.0.

When evaluating the function of Eq(7.18), one must be cognizant that the polychromatic nature of the X-Ray radiation and the tube's energy dependent efficiency are not considered (along with other factors), and therefore the relationship provides only the fundamental guidelines associated with understanding the voltage regulation requirements, and the trends associated with its sensitivities.

7.4 Sensitivity to X-Ray Tube Beam Intensity Variations

For a fixed X-Ray Tube potential, or when considering the Curie (Ci) rating of an Isotope source (μ or q effectively constant), the relative variation in the intensity of the generator / source emitted radiation can be characterized from Eq(7.2).

$$\frac{\partial x}{x} = -\left(\frac{\rho}{\mu}\right)\frac{1}{\rho x}\frac{\partial I}{I} = -\frac{1}{\mu x}\frac{\partial I}{I} = -\frac{q}{x}\frac{\partial I}{I} = -\frac{q}{x}\frac{\partial I_0}{I_0} \tag{7.19a}$$

or

$$\frac{\Delta x}{x} = -\left(\frac{\rho}{\mu}\right)\frac{1}{\rho x}\frac{\Delta I_0}{I_0} = -\frac{q}{x}\frac{\Delta I_0}{I_0} \tag{7.19b}$$

Isotope source variations are dominated by Poisson statistics, and therefore the characteristics of the associated relative measurement noise are also dictated by these statistics. In X-Rays, due to the fundamental physics of the escape of thermally excited filament electrons, the noise characteristics involve a certain amount of Shot Noise. The reciprocal behavior of the MAC / MFP provides an attenuation for larger thicknesses, while thicknesses below an MFP of 1.0 while experience amplified noise levels.

7.5 Sensitivity to Variations in Material Composition

To render an accurate thickness measurement, radiation absorption gauges require a knowledge of material's radiation attenuation characteristics (i.e., (μ/ρ), ρ or q). These parameters can be obtained by direct calibration with samples of known thickness and

composition, or through direct entry of the chemical / elemental constituents and their associated percentage inclusions (coupled with tabulated listings of the MACs (Hubble & Seltzer, 2004)). Failure to properly characterize the attenuation parameters of the material under measurement will lead to an improper set-up of the instrument's operating point and inaccurate indications of the material thickness.

To examine the instrument's sensitivity to variances in the alloy of the material, we will examine a case where an alloy of known chemistry and density, is subject to contamination by a low level concentration of a non-accounted constituent.

Constituent #1 – Base alloy (of possibly many components) that is known to the gauge.

Constituent #2 – Contaminating component of *unknown* attenuation characteristics, density and concentration / weighting.

If we assume that the material's constituent attenuation behavior can be characterized as a composition of successive layers of the various elements. The actual thickness, X, is therefore the sum of the individual layer thicknesses.

$$X = x_1 + x_2 \quad \Rightarrow \quad X = \sum_{i=1}^{N} x_i \tag{7.20}$$

The attenuated beam intensity emitted from each layer is given by:

$$I_1 = I_0 e^{-\frac{x_1}{q_1}} \tag{7.21a}$$

$$I_2 = I_1 e^{-\frac{x_2}{q_2}} \tag{7.21b}$$

$$\Downarrow$$

$$I = I_N = I_{N-1} e^{-\frac{x_N}{q_N}} \tag{7.21c}$$

or

$$I = I_0 \left[e^{-\frac{x_1}{q_1}} \cdot e^{-\frac{x_2}{q_2}} \right] \quad \Rightarrow \quad I = I_0 \left[e^{-\frac{x_1}{q_1}} \cdot e^{-\frac{x_2}{q_2}} \cdot \cdots \cdot e^{-\frac{x_N}{q_N}} \right] \tag{7.22}$$

The erroneous, measured thickness reading from the gauging system, X_m, is based on the assumption that the material is only composed of the q_1 constituent attenuation.

$$I = I_0 e^{-\frac{X}{q_A}} = I_0 e^{-\frac{X_M}{q_1}} \tag{7.23}$$

where q_A is the composite MFP. Understanding the nature of the differences between Eq(7.23) and Eq(7.22) is key to assessing the sensitivity to alloy variations. The relationship between the actual and measured thickness is based on:

$$I = I_0 \left[e^{-\frac{X}{q_A}} \right] = I_0 \left[e^{-\frac{x_1}{q_1}} \cdot e^{-\frac{x_2}{q_2}} \right] = I_0 \left[e^{-\frac{X_M}{q_1}} \right] \tag{7.24}$$

$$-\ln\left[\frac{I}{I_0}\right]=\frac{X}{q_A}=\frac{x_1}{q_1}+\frac{x_2}{q_2}=\frac{X_M}{q_1} \quad \Rightarrow \quad \frac{x_1}{q_1}+\frac{x_2}{q_2}+\cdots+\frac{x_N}{q_N}=\frac{X_M}{q_1} \tag{7.25}$$

or

$$X_M=q_1\left[\frac{x_1}{q_1}+\frac{x_2}{q_2}\right] \quad \Rightarrow \quad X_M=q_1\left[\frac{x_1}{q_1}+\frac{x_2}{q_2}+\cdots+\frac{x_N}{q_N}\right] \tag{7.26}$$

The relationship between the actual thickness, X, and the measured thickness, X_m, is:

$$X=x_1+x_2=K_qX_M \quad \Rightarrow \quad X=\sum_{i=1}^{N}x_i=K_qX_M \tag{7.27}$$

Therefore from Eq(7.25)

$$K_q=\frac{q_A}{q_1}=\frac{x_1+x_2}{q_1\left[\frac{x_1}{q_1}+\frac{x_2}{q_2}\right]} \quad \Rightarrow \quad K_q=\frac{q_A}{q_1}=\frac{\sum_{i=1}^{N}x_i}{q_1\left[\sum_{i=1}^{N}\frac{x_i}{q_i}\right]} \tag{7.28}$$

which provides the composite MFP, q_A as:

$$q_A=\frac{x_1+x_2}{\left[\frac{x_1}{q_1}+\frac{x_2}{q_2}\right]} \quad \Rightarrow \quad q_A=\frac{\sum_{i=1}^{N}x_i}{\left[\sum_{i=1}^{N}\frac{x_i}{q_i}\right]} \tag{7.29}$$

Considering our two(2) constituent example, the component weighting follows from Eqs(4.4a,b) and Eq(4.5), and is based on convex function of the alloy inclusion, α.

$$w_1=(1-\alpha)=\frac{\rho_1x_1}{\rho_AX} \tag{7.30a}$$

$$w_2=\alpha=\frac{\rho_2x_2}{\rho_AX} \tag{7.30b}$$

where ρ_A is the composite density of the total alloyed material and it is assumed that the alloy inclusion is small (i.e., $\alpha\to 0$). Rearranging Eq(7.30a) results in:

$$x_1=w_1\frac{\rho_AX}{\rho_1} \quad \Rightarrow \quad x_i=w_i\frac{\rho_AX}{\rho_i} \tag{7.31}$$

Returning to Eq(7.28), we have:

$$K_q = \frac{\frac{w_1}{\rho_1} + \frac{w_2}{\rho_2}}{q_1\left[\frac{w_1}{\rho_1 \cdot q_1} + \frac{w_2}{\rho_2 \cdot q_2}\right]} = \frac{\frac{w_1}{\rho_1} + \frac{w_2}{\rho_2}}{q_1\left[w_1\left(\frac{\mu}{\rho}\right)_1 + w_2\left(\frac{\mu}{\rho}\right)_2\right]} \tag{7.32a}$$

$$\Downarrow$$

$$K_q = \frac{\sum_{i=1}^{N}\frac{w_i}{\rho_i}}{q_1\left[\sum_{i=1}^{N}\frac{w_i}{\rho_i \cdot q_i}\right]} = \frac{\sum_{i=1}^{N}\frac{w_i}{\rho_i}}{q_1\left[\sum_{i=1}^{N} w_i\left(\frac{\mu}{\rho}\right)_i\right]} \tag{7.32b}$$

which provides the composite MFP, q_A as:

$$q_A = \frac{\frac{w_1}{\rho_1} + \frac{w_2}{\rho_2}}{\left[w_1\left(\frac{\mu}{\rho}\right)_1 + w_2\left(\frac{\mu}{\rho}\right)_2\right]} = \frac{\left[\frac{(1-\alpha)}{\rho_1} + \frac{\alpha}{\rho_2}\right]}{\left[(1-\alpha)\left(\frac{\mu}{\rho}\right)_1 + \alpha\left(\frac{\mu}{\rho}\right)_2\right]} \quad \Rightarrow \quad q_A = \frac{\sum_{i=1}^{N}\frac{w_i}{\rho_i}}{\left[\sum_{i=1}^{N} w_i\left(\frac{\mu}{\rho}\right)_i\right]} \tag{7.33}$$

It is important to note that the above formulations assume that the volume of the composite alloy equals the sum of the volume of the constituents (prior to mixing).

The real problem at hand is determining if a change in the transmitted radiation, I, is the result of a change in the actual thickness, X, or a change in composition, which can be examined through the fundamental relationship of Eq(7.25).

$$\frac{X}{q_A} = X\frac{\left[(1-\alpha)\left(\frac{\mu}{\rho}\right)_1 + \alpha\left(\frac{\mu}{\rho}\right)_2\right]}{\left[\frac{(1-\alpha)}{\rho_1} + \frac{\alpha}{\rho_2}\right]} \tag{7.34}$$

We are interested in obtaining the relative error as a function of variations in the alloy inclusion, α. Variations in the received radiation intensity due to variations in actual thickness or to variations in the alloy inclusion are related by:

$$\frac{\partial\left(\frac{X}{q_A}\right)}{\partial X}\partial X = \frac{\partial\left(\frac{X}{q_A}\right)}{\partial \alpha}\partial\alpha \tag{7.35}$$

which results in:

$$\frac{\left[(1-\alpha)\left(\frac{\mu}{\rho}\right)_1+\alpha\left(\frac{\mu}{\rho}\right)_2\right]}{\left[\frac{(1-\alpha)}{\rho_1}+\frac{\alpha}{\rho_2}\right]}\partial X=\cdots$$

$$=\left[\frac{\left[\frac{(1-\alpha)}{\rho_1}+\frac{\alpha}{\rho_2}\right]\left[\left(\frac{\mu}{\rho}\right)_2-\left(\frac{\mu}{\rho}\right)_1\right]-\left[(1-\alpha)\left(\frac{\mu}{\rho}\right)_1+\alpha\left(\frac{\mu}{\rho}\right)_2\right]\left[\frac{1}{\rho_2}-\frac{1}{\rho_1}\right]}{\left[\frac{(1-\alpha)}{\rho_1}+\frac{\alpha}{\rho_2}\right]^2}\right]X\,\partial\alpha \quad (7.36)$$

Since the alloy inclusion, α, is small

$$\frac{\partial X}{X}=\left[\frac{\left[\frac{1}{\rho_1}+\frac{\alpha}{\rho_2}\right]\left[\left(\frac{\mu}{\rho}\right)_2-\left(\frac{\mu}{\rho}\right)_1\right]-\left[\left(\frac{\mu}{\rho}\right)_1+\alpha\left(\frac{\mu}{\rho}\right)_2\right]\left[\frac{1}{\rho_2}-\frac{1}{\rho_1}\right]}{\left[\frac{1}{\rho_1}+\frac{\alpha}{\rho_2}\right]\left[\left(\frac{\mu}{\rho}\right)_1+\alpha\left(\frac{\mu}{\rho}\right)_2\right]}\right]\partial\alpha \quad (7.37)$$

which reduces to :

$$\frac{\partial X}{X}=\left[\frac{\left[\left(\frac{\mu}{\rho}\right)_2-\left(\frac{\mu}{\rho}\right)_1\right]}{\left[\left(\frac{\mu}{\rho}\right)_1+\alpha\left(\frac{\mu}{\rho}\right)_2\right]}+\left[\frac{\rho_2-\rho_1}{\rho_2+\alpha\rho_1}\right]\right]\partial\alpha \quad (7.38a)$$

or

$$\frac{\Delta X}{X}=\left[\frac{\left[\left(\frac{\mu}{\rho}\right)_2-\left(\frac{\mu}{\rho}\right)_1\right]}{\left[\left(\frac{\mu}{\rho}\right)_1+\alpha\left(\frac{\mu}{\rho}\right)_2\right]}+\left[\frac{\rho_2-\rho_1}{\rho_2+\alpha\rho_1}\right]\right]\Delta\alpha \quad (7.38b)$$

A key factor in Eq(7.38) is that the impact of the alloy inclusion is separable in terms of the differences in MACs and in densities. This is important, since the MAC terms are functions of the applied radiation's spectral content, while the density and alloy inclusion remain independent of radiation.

In an X-Ray System, the applied tube potential can be swept across an energy range, while relative sensitivity measurements are made. From these measurements it is possible to identify the differential MAC components, and infer the density difference from projections to a nominal, zero thickness offset. In the bi-alloy case of Eq(7.38b), it is possible to take two(2) measurements at strategically different energies (i.e., tube voltages that yield sufficiently different values of MACs), and resolve two(2) independent equations and two(2) unknowns (the unknowns being the actual thickness, X, and the alloy inclusion, α).

7.6 Sensitivity to Variations in Pass-Line Height

Variations in the vertical location of the material can introduce measurement errors. These primarily stem from the geometries of the radiation lobe patterns associated with coherent and incoherent scattering (see Section 4.2). As shown in Figure 4.1, within the radiation energy region of interest (10keV to 200keV), the MAC is composed of photoelectric absorption, coherent and incoherent scattering. As radiation energy levels approach and exceed 100keV, the nature of the transmitted radiation shifts from a photoelectric absorption to an incoherent scattering form (Compton).

As shown in Figure 7.4a, the generated radiation beam is formed about the optical axis, with conic angles defined by the point-size of the source, and the size, orientation and location of the collimating aperture. The transmitted beam, emerging from the strip, tends to maintain the conic angle relationship and is ultimately over-contained by the detector. A component of the radiation emerging from the strip is associated with scattering. The radiation pattern forms in lobes about the optical axis, largely directed about a primary / dominant scattering angle.

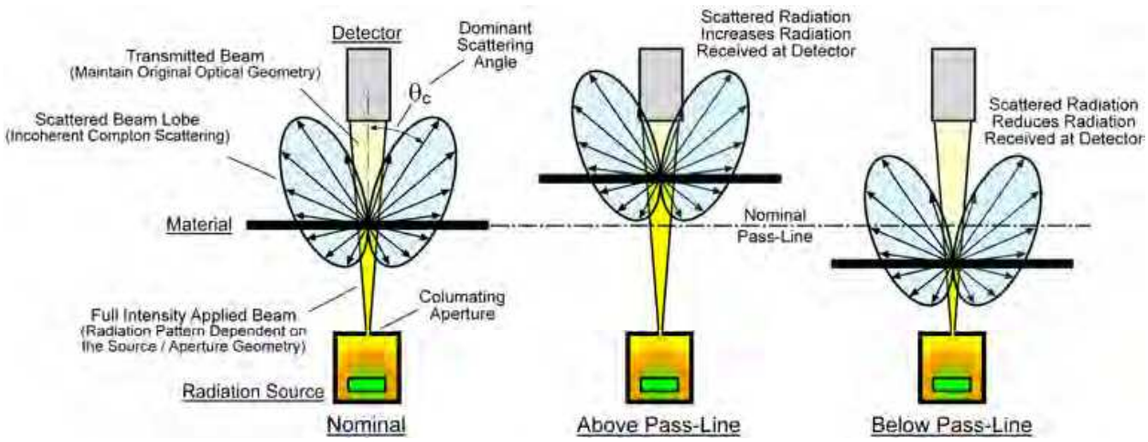

Fig. 7.4 – Illustration of the radiation pattern geometry and impact on measurement accuracy in the presence of pass-line height variations: a) Definition of the radiation patters, including the primary transmitted beam and incoherent scattering (Compton) lobe patterns, b) Exaggerated illustration of the impact of a vertical offset in pass-line height, c) Exaggerated illustration of the impact of a vertical reduction in pass-line height.

At pass-line heights above the nominal (see Figure 7.4b), the geometry of the scattered radiation pattern causes the detector's received radiation intensity to increase, inducing the instrument to report a thinner than actual reading. Measurement errors can approach 0.1% of the nominal thickness for 10mm of pass-line height change when the air gap distances are small and the radiation source collimator projects a wide angled beam.

At pass-line heights below the nominal (see Figure 7.4c), the geometry of the scattered radiation pattern directs too many photons away from the detector. Depending on the extent of the nominal pass-line scattering characteristics, the detector's received radiation intensity may potentially decrease, inducing the instrument to report a thicker than actual reading, or may show no response.

When the air gap distance is relatively large >150mm, and the beam angle is relatively tight, the pass-line height variations are not significant for normal operating conditions on properly aligned equipment. Certain cold mill wiping systems can modify the pass-line height introducing the possibility for measurement errors on small air gap isotope gauges mounted close to the wiping systems.

When X-Ray Systems are operated at higher energies (>100kV), the transmitted radiation is dominated by Compton Scattering, making these systems (and operating regimes) more susceptible to pass-line elevation induced measurement errors.

7.7 Sensitivity to Variations in Pass-Line Inclination

Changes to the angle of the material presented to the radiation beam can result in measurement errors due to the oblique angle of incidence. These errors are associated with the cosine effects leading to a longer pathway through the material. Figure 7.5 illustrates this condition.

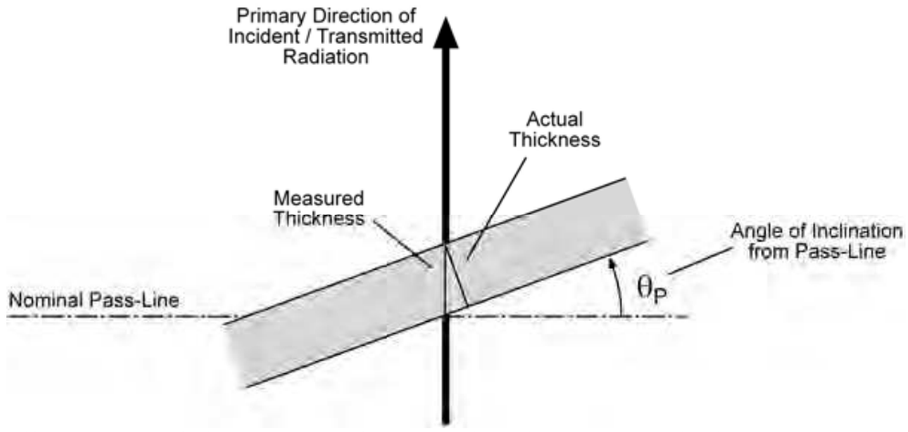

Fig. 7.5 – Illustration of the impact of material inclination, with the increased path-length associated the cosine effect.

The impact on the measured thickness, X_M, for an actual thickness, X, is given by:

$$X_M = \frac{X}{\mathrm{Cos}(\theta_P)} \tag{7.39}$$

where θ_P is the angle of material inclination for the reference pass-line. The longer pathway cause the instrument to report a thicker than actual reading.

It's important to note that combinations of pass-line height and inclination variations can induce complex measurement errors. This is primarily evident when rolling / measuring relatively thick / heavy gauge plate materials (~10-15mm) having center-buckling flatness distortions. These longitudinal waves induce both pass-line height and inclination angle variations, as the strip passes, causing oscillating measurement errors.

7.8 Sensitivity to Variations in Air Gap Temperature and Density

The ambient atmosphere above and below the material, within the air column about the optical axis in the air gap, is also involved in the attenuation of the applied and transmitted / scattered radiation, and therefore the instruments measurements. The composite MAC for air coupled with the instantaneous density of the air column, form the air gap's attenuation characteristics.

Changes in the air gap, air column temperature cause a direct change in the air column density, resulting in a measurement error. This is most apparent when measuring thin materials or materials having reduced absorption characteristics. The general trends are as follows:

- Increases in Air Column Temperature result in a reduction of the air column density, allowing more radiation to pass and be collected by the detector. The instrument will report a thinner than actual reading.
- Decreases in Air Column Temperature result in an increase of the air column density, attenuating more radiation and reducing the radiation collected by the detector. The instrument will report a thicker than actual reading.

Returning to the attenuation equations of Eq(6.2) and Eq(7.25), the actual measurement situation can be more precisely described by:

$$-\ln\left[\frac{I}{I_0}\right] = \frac{X}{q} + \frac{Z}{q_{AG}} = \frac{X_M}{q_S} \tag{7.40}$$

where Z is the air gap dimension, q is the MFP of the material, q_{AG} is the air column MFP and q_s is the effective MFP determined during the last standardization. Variations in the received radiation intensity due to variations in actual thickness or to variations in the air gap attenuation characteristics are related by:

$$\frac{\partial\left(\frac{X_M}{q_S}\right)}{\partial X}\partial X = \frac{\partial\left(\frac{X_M}{q_S}\right)}{\partial q_{AG}}\partial q_{AG} \tag{7.41}$$

which results in:

$$\frac{1}{q}\partial X = -\frac{Z}{\left(q_{AG}\right)^2}\partial q_{AG} \tag{7.42}$$

The variation in thickness which would result from variation in the air gap attenuation is given by:

$$\partial X = -\frac{Z \cdot q}{\left(q_{AG}\right)^2}\partial q_{AG} \tag{7.43}$$

If we consider only monochromatic radiation, the MFP of the air gap, q_{AG}, is related to the average distance between atoms in the air column gasses. For a mass of gas held at the same pressure, we have:

$$\frac{\partial V}{V} = \frac{\partial T_{AG}}{T_{AG}} \tag{7.44}$$

where V is the volume of the gas mass, and T_{AG} is the gas temperature. Since the volume, mass, density and MFP of the air column gas are related, we can use:

$$\frac{\partial q_{AG}}{q_{AG}} = \frac{\partial T_{AG}}{T_{AG}} \tag{7.45}$$

Returning to Eq(7.43), results in:

$$\partial X = -Z \cdot \frac{q}{q_{AG} \cdot T_{AG}} \partial T_{AG} = -Z \cdot \frac{\left(\frac{\rho}{\mu}\right)\frac{1}{\rho}}{\left(\frac{\rho}{\mu}\right)_{AG} \frac{1}{\rho_{AG}(T_{AG})} \cdot T_{AG}} \partial T_{AG} \tag{7.46a}$$

or

$$\Delta X = -Z \cdot \frac{q}{q_{AG} \cdot T_{AG}} \Delta T_{AG} = -Z \cdot \frac{\left(\frac{\mu}{\rho}\right)_{AG}}{\left(\frac{\mu}{\rho}\right)} \frac{\rho}{\rho_{AG}(T_{AG})} \frac{\Delta T_{AG}}{T_{AG}} \tag{7.46b}$$

It is important to note MACs of the material and air gap column are constant, and not function of density or temperature. The density of the air gap gasses, $\rho_{AG}(T_{AG})$ is a function of temperature, and has a reciprocal relationship within this function, causing an increase in the measurement error as the density is reduced with temperature.

At 20 deg C, an increase in the air gap temperature of 30 deg C at 60% humidity, has a 12.1% reduction in the air density, which can have a dramatic effect on the instrument's behavior. Depending on the radiation energy level and the material chemistry, this level of air density variation can create measurement errors on the order of 0.15% of the nominal thickness.

7.9 Sensitivity to Variations in Material Temperature

Transmission based radiation thickness gauges measure the mass per unit area of the material in the beam. At an elevated temperature, T_1, the material volume increases, causing the unit area of the material engaged with the radiation beam to be reduced (when considering its ambient temperature conditions, T_0). Therefore, the area engaged, A_0, with the beam at the ambient temperature T_0, will expand to the area, A_1, at the material temperature, T_1, in the following manner:

$$A_1 = A_0\left(1 + 2K_T\left(T_1 - T_0\right)\right) \tag{7.47}$$

where K_T is the 1st order thermal expansion coefficient of the material (neglecting higher order terms). Therefore, a measurement taken at a material temperature of T_1, should be adjusted for a final ambient temperature of T_0, in the following manner:

$$X_M\big|_{T_0} = X_M\big|_{T_1} \cdot \left(1 + 2K_T\left(T_1 - T_0\right)\right) \tag{7.48}$$

7.10 Sensitivity to Variations in the Integration Time Period (Time Constants)

As shown in Section 7.2, the system's absolute statistical noise is described by Eq(7.10), where it is noted that the integration time, $\Delta\tau$, appears as a reciprocal of the square root:

$$\Delta x = f\left(\frac{1}{\sqrt{\Delta\tau}}\right) \tag{7.49}$$

The system integration time and response time constant are typically programmable parameters that can be adjusted to improve the system noise levels / performance. Due to the relationships of Eq(7.10) and Eq(7.49), the adjustments to the integration time / time constants can be described by:

$$\Delta x\big|_{\Delta\tau_2} = \Delta x\big|_{\Delta\tau_1}\sqrt{\frac{\Delta\tau_1}{\Delta\tau_2}} \tag{7.50}$$

where

$\Delta x\big|_{\Delta\tau_1}$ & $\Delta x\big|_{\Delta\tau_2}$ - Absolute statistical noise levels with integration times, $\Delta\tau_1$ & $\Delta\tau_2$.

$\Delta\tau_1$ & $\Delta\tau_2$ - Different integration times

Often, the final time constant / integration time of the system is defined by the application, and therefore noise reduction methods involving this approach may not be available.

8. Architecture of Thickness Measurement Systems

Figure 2.1 provides a base-line overview of the primary components associated with a typical thickness measurement system. Figure 8.1 expands on this representation and partitions the components to their classical physical locations.

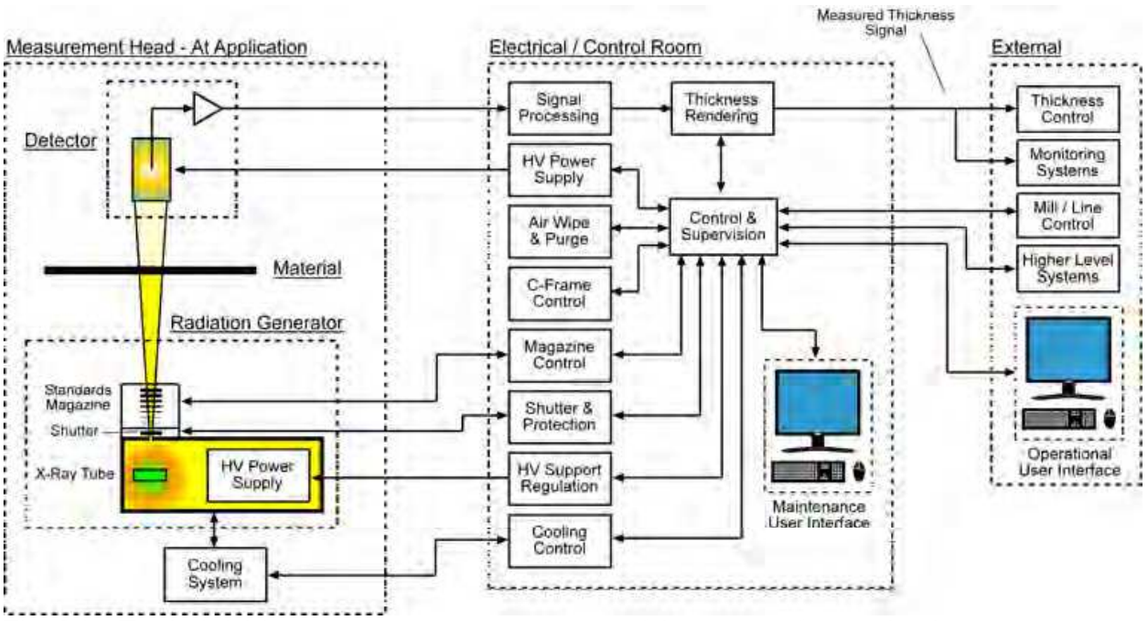

Fig. 8.1 – Typical thickness measurement system architecture and organization.

The key factor in the Figure 8.1 arrangement are the centralization of signal processing and control to a possibly remote location (Electrical Control Room). This suggests long, potentially noise corrupted signal runs, however this arrangement is commonplace in many existing legacy class systems currently in operation.
Modern systems employ highly networked arrangements to support high speed data sets and allow interfacing to a broader array of process related systems (Zipf, et. al., 2007). Figure 8.2 provides a network hierarchical view of a typical system networked interconnect for rolling mill applications.

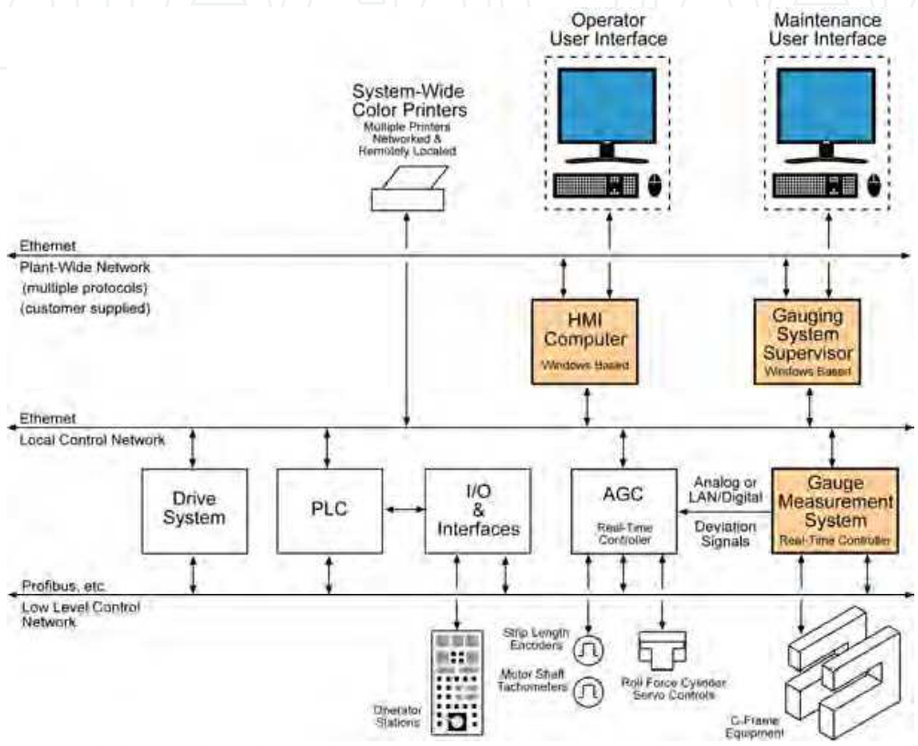

Fig. 8.2 – Network hierarchy of a multi-subsystem interconnect for applications to rolling mills.

9. System Implementations

When considering flat strip / sheet processing, there are a number of thickness measurement interests, including: longitudinal center-line thickness (along the length) as opposed to the transverse thickness profile (along the width). Some implementations may allow the measurement head (detector / radiation generator pair) to be retracted off-line, while others provide only fixed mounting locations. It all depends on the nature of the desired measurement.

9.1 Classical Measuring Head Configurations

A classical measuring head configuration is the C-Frame, shown in Figure 8.1, where the radiation generator is located beneath the strip and the detector above (I2S, 1992). This arrangement has sufficient structural stability to maintain proper alignment of the detector along the optical axis of the radiation generator. It also provides a convenient means of

engaging the strip and retracting the unit off-line. The depth of the C-Frame throat can be manufactured to provide full strip width profiling and full extension across the strip for easy maintenance access.

(a) (b)

Fig. 8.1 – Photo diagrams showing various C-Frame arrangements: a) Primary components, b) C-Frame in flat strip application.

Other common mounting arrangements include O-Frames (that completely encompass the strip width) and Fixed Locations (generator and detector are physically mounted in place).

9.2 Measurement Plans

The application dictates the location and dynamics of the thickness measurement on the strip. Figure 8.2 illustrates some typical measurement plans.

Fixed mounting locations (Figure 8.2a) are uncommon, but necessary when the mechanical structures / surroundings of the application do not provide sufficient space for the mounting of retractable C-Frame equipment and support systems. This arrangement not only has a fixed measurement (typically strip center-line), but also can present difficulties in accessing the components for maintenance and repair. One point of advantage is that this arrangement can afford substantial protective enclosures / guarding, making the equipment essentially impervious to damage from process abnormalities (e.g., strip breaks, mill wrecks, etc.).

Retractable arrangements (Figure 8.2b) are perhaps the most common. These offer the ability to withdraw the C-Frame off-line (for maintenance and repair access), but only provide center-line or rear strip edge measurement capabilities.

Profiling C-Frame arrangements (Figure 8.2c) are the most versatile. They offer the ability to measure at any location across the transverse strip width (including center-line), and can be used to obtain transverse strip profile measurements. The deep C-Frame throat also allows these gauging systems to be traversed fully across the strip, for easy access to the detector and radiation generator equipment.
Dual C-Frame arrangements (Figure 8.2d) are uncommon. They are considered only in applications where simultaneous strip center-line and profile measurements must be provided. Often the center-line measurement is provided to thickness control systems, while the strip profile measurements are provided for quality control monitoring purposes.

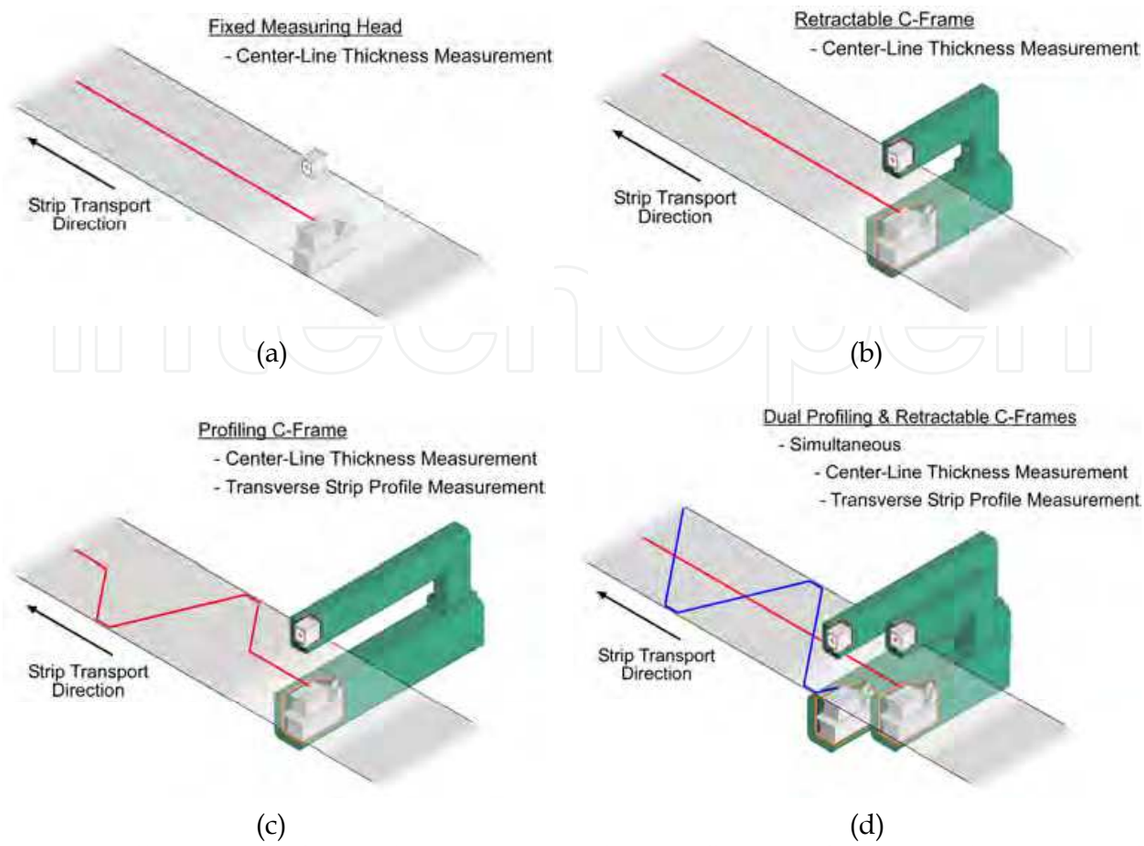

Fig. 8.2 – Illustrations of typical measurement plans on flat strip / sheet products: a) Fixed Measuring Head, b) Retractable C-Frame, c) Profiling C-Frame, d) Dual Profiling & Retractable C-Frames.

10. Conclusion

This chapter has explored the underlying physics and methods associated with radiation based measurements of material thickness. The intent of this chapter has been to provide a tutorial foundation of these principles, to support subsequent discussions (Zipf, 2010). The primary components of this form of measurement system have been presented and discussed. Natural and artificial radiation sources / generators have been examined and considered for application. The nature of the material's interaction with radiation is analyzed and considered in the presence of possibly complex material chemistries have been identified and accommodated in the methods for rendering a measurement. Detection system sensors and instrumentation have been presented and evaluated with respect to their employment in these measurement systems. The typical signal processing flow has been reviewed, along with the manner in which the measurement is resolved and distributed to external systems. A sensitivity analysis has been provided to identify key parameters and relationships that influence the quality, accuracy and precision of the measurement signal. Classical system architectures and implementations have been presented and discussed.

11. References

Bose, N. (1985). *Digital Filters – Theory and Applications*, Elsevier Scientific Publishing Co., ISBN 0-444-00980-9, New York, NY

Cooper, W. (1978). *Electronic Instrumentation and Measurement Techniques* - 2nd Edition, Prentice-Hall, Inc., ISBN 0-13-251710-8, Englewood Cliffs, NJ

Graydon, A. (1950). *Dissociation Energies and Spectra of Diatomic Molecules*, Dover Publishing, Inc., New York, NY

Halliday, D. (1955). *Introductory Nuclear Physics*, John Willey & Sons, Inc., Library of Congress Catalog Card Number : 55-9365, New York, NY

Harting, E. & Read, F. (1976). *Electrostatic Lenses*, Elsevier Scientific Publishing Co., ISBN 0-444-41319-7, Amsterdam, The Netherlands

Howard, R. (1970). Recent Advances in High-Speed X-Ray Thickness Gaging of Steel Strip, *Transactions of the Instrument Society of America*, Vol. 9, No. 4, (1970), pp. 348-354.

Hubble, J. & Seltzer, S. (2004). Tables of X-Ray Mass Attenuation Coefficients and Mass Energy-Absorption Coefficients (version 1.4), National Institute of Standards and Technology, Gaithersburg, MD

I2S – Intergrated Industrial Systems, Inc. (1992), *Gauge Signal Processing Unit Manual*, Intergrated Industrial Systems, Inc., Yalesville, CT

I2S – Intergrated Industrial Systems, Inc. (2004), *X-Ray Gauging System – Time Domain Response Analysis*, Technical Report : 040229 v1.3, Intergrated Industrial Systems, Inc., Yalesville, CT

IEC (1996). Nuclear Instrumentation – Thickness Measurement Systems Utilizing Ionization Radiation : Definitions and Test Methods, IEC-1336 (1996), International Electrotechnical Commission.

Kaplan, I. (1955). *Nuclear Physics*, Addison-Wesley Publishing Co., Library of Congress Catalog Card Number : 54-5732, Reading, MA

Kraus, J. & Carver, K. (1973). *Electromagnetics*, McGraw-Hill Book Co., ISBN 0-07-035396-4, New York, NY

Letokhav, V. (1987). *Laser Photoionization Spectroscopy*, Academic Press, Inc., ISBN 0-12-444320-6, Orlando, FL

Mark, T. & Dunn, G. (1985). *Electron Impact Ionization*, Springer-Verlag, ISBN 3-211-81778-6, Vienna, Austria

Moore, J., Davis, C. & Coplan, M. (1983). *Building Scientific Apparatus*, Addison-Wesley Publishing Co., ISBN 0-201-05532-5, London, England

Motchenbacher, C. & Fitchen, F. (1973). *Low-Noise Electronic Design*, John Willey & Sons, Inc., ISBN 0-471-61950-7, New York, NY

Nyce, D. (2004). *Linear Position Sensors - Theory and Application*, John Wiley & Sons, ISBN 978-0-471-23326-8, New York, NY

RCA – Radio Corporation of America, (1963). *Phototubes and Photocells – Technical Manual PT-60*, Radio Corportation of America, Lancaster, PA

Zipf, M. (2010). Radiation Transmissoin-based Thickness Measurement Systems – Advancement, Innovations and New Technologies, In: *Advances in Measurement Systems*, Chapter 7, Kordic, V. (Ed), In-Tech Publications, Vienna, Austria

Zipf, M., Hummel, C. & Burgess, R. (2007). A New Automation Architecture for Strip Thickness Gauging Systems, *Proceedings of the Associação Brasileira de Metalurgia e Materiais, 44th Rolling Seminar – Processes, Rolled and Coated Products*, Campos do Jordao, SP, Brazil, October 16-19, 2007, Campos do Jordao, SP, Brazil, Associação Brasileira de Metalurgia e Materiais, Sao Paulo, Brazil

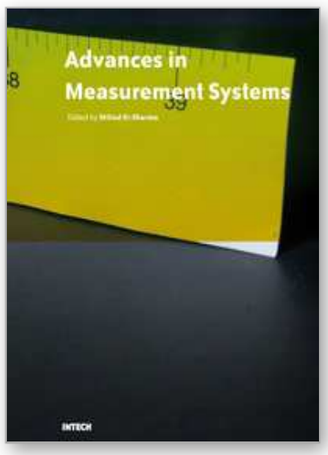

Advances in Measurement Systems

Edited by Milind Kr Sharma

ISBN 978-953-307-061-2
Hard cover, 592 pages
Publisher InTech
Published online 01, April, 2010
Published in print edition April, 2010

How to reference

In order to correctly reference this scholarly work, feel free to copy and paste the following:

Mark E. Zipf (2010). Radiation Transmission-based Thickness Measurement Systems - Theory and Applications to Flat Rolled Strip Products, Advances in Measurement Systems, Milind Kr Sharma (Ed.), ISBN: 978-953-307-061-2, InTech, Available from: http://www.intechopen.com/books/advances-in-measurement-systems/radiation-transmission-based-thickness-measurement-systems-theory-and-applications-to-flat-rolled-st

INTECH
open science | open minds

InTech Europe
University Campus STeP Ri
Slavka Krautzeka 83/A
51000 Rijeka, Croatia
Phone: +385 (51) 770 447
Fax: +385 (51) 686 166
www.intechopen.com

InTech China
Unit 405, Office Block, Hotel Equatorial Shanghai
No.65, Yan An Road (West), Shanghai, 200040, China
中国上海市延安西路65号上海国际贵都大饭店办公楼405单元
Phone: +86-21-62489820
Fax: +86-21-62489821

IntechOpen